Journal of Geophysical Research: Earth Surface

RESEARCH ARTICLE
10.1029/2018JF004718

Growing Forced Bars Determine Nonideal Estuary Planform

J. R. F. W. Leuven[1], L. Braat[1], W. M. van Dijk[1], T. de Haas[1], E. P. van Onselen[1], B. G. Ruessink[1], and M. G. Kleinhans[1]

[1] Faculty of Geosciences, Utrecht University, Utrecht, Netherlands

Key Points:
- Quasiperiodic estuary planforms arise from diversion of flow around forced nonmigratory midchannel bars that causes bank erosion
- Self-formed confinements separate zones in which the estuary is wider and bars are more dynamic
- Confinement spacing scales with bar dimensions and estuary width in experiments and nature

Supporting Information:
- Supporting Information S1
- Movie S1

Correspondence to:
J. Leuven,
j.r.f.w.leuven@uu.nl

Citation:
Leuven, J. R. F. W., Braat, L., van Dijk, W. M., de Haas, T., van Onselen, E. P., Ruessink, B. G., & Kleinhans, M. G. (2018). Growing forced bars determine nonideal estuary planform. *Journal of Geophysical Research: Earth Surface*, *123*. https://doi.org/10.1029/2018JF004718

Received 22 APR 2018
Accepted 7 OCT 2018
Accepted article online 13 OCT 2018

Abstract The planform of estuaries is often described with an ideal shape, which exponentially converges in landward direction. We show how growing topographically forced nonmigratory (i.e., anchored) bars determine the large-scale estuary planform, which explains the deviations observed in the planform of natural estuaries filled with bars compared to the ideal planform. Experiments were conducted in a 20-m long, 3-m-wide tilting flume, the Metronome. From a narrow, converging channel a self-formed estuary developed characterized by multiple channels, braided bars, a meandering ebb channel, and an ebb delta. Bars hardly migrated due to the alternating current, but the bar width increased with increasing estuary width. At locations where the estuary width was narrow, major channel confluences were present, while the zones between the confluences were characterized by a higher braiding index, periodically migrating channels, and a relatively large estuary width. At the seaward boundary, confluences were forced in place by the presence of the ebb tidal delta. Between confluences, bars were topographically forced to be nonmigratory. Diversion of flow around forced midchannel bars caused bank erosion. This resulted in a planform shape with a quasiperiodic widening and narrowing at the scale of forced bars. Observations in natural systems show that major confluence locations can also be caused by inherited geology and human engineering, but otherwise the estuary outline is similarly affected by tidal bars. These observations provide a framework for understanding the evolution of tidal bar patterns and the planform shape of the estuary, which has wide implications for navigation, dredging, and ecology.

Plain Language Summary Estuaries, which are also called river mouths, form the transition from rivers to the ocean. A common concept to describe the shape of these tidally influenced estuaries is the concept of an ideal estuary, which describes estuaries as perfectly converging channels. However, in natural systems we often observe planform shapes that deviate from this converging shape. In this article, we show with experiments in a tilting flume that estuaries without any hard boundaries (such as bedrock geology) evolve into planforms with an irregular shape rather than the perfectly converging shape. We identified a mechanism in which sand bars build up in the center of the estuary, after which the flow is diverted around the bars. This process results in local widening where tidal bars initially formed, while the estuary remains relatively narrow at zones between the bars. This mechanism helps to understand the dynamic behavior of estuaries, in which bars form valuable ecological habitat and in which channels provide access to million dollar harbors.

1. Introduction

Estuaries are tidal systems that occur where rivers debouch into the sea. The planform of estuaries is often described by an ideal shape (Langbein, 1963; Pillsbury, 1956; Savenije, 2015), which is defined as an equilibrium state wherein the channel planform converges with a constant along-channel tidal range, average depth, and current velocity amplitude. The imposed landward decrease in tidal prism has a first-order control on the planform shape, resulting in converging (*funnel-shaped*) channels for delta branches and tidal creeks. However, previous research showed that in alluvial estuaries a second-order complexity is superimposed on the converging shape, which results in more irregular planforms with locally widened zones (Leuven, de Haas, et al., 2018; Figure 1). Deviations from the ideal shape may occur because the estuary adapted in varying degrees to its equilibrium shape, depending on the time and sediment available to adapt to changing boundary conditions, such as Holocene sea level rise and antecedent topography (de Haas et al., 2017; Townend, 2012). In addition, the outline may be shaped by external restrictions that impose local confinements, such as inherited geology or human engineering, as well as self-formed restrictions, such as salt marshes and riparian

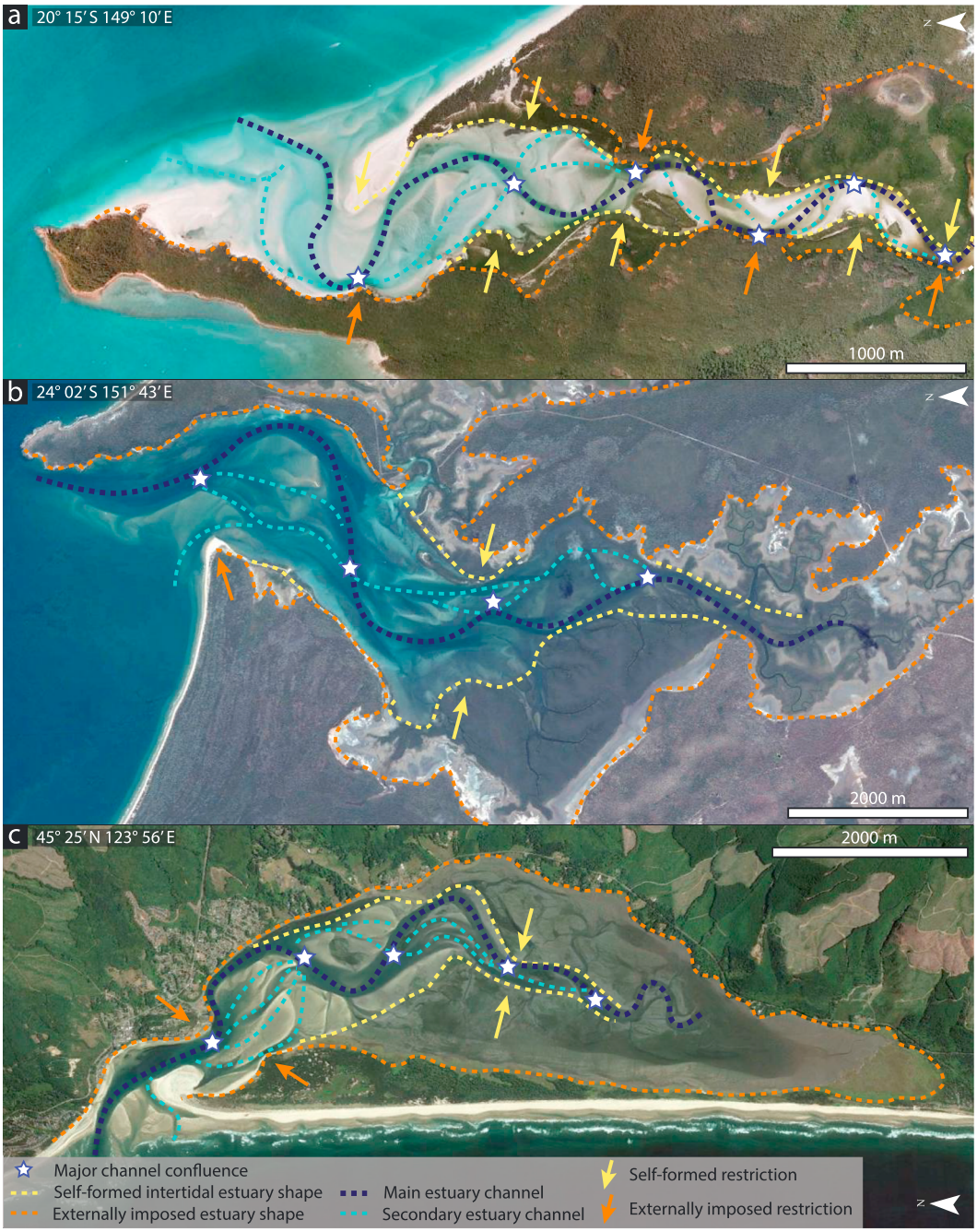

Figure 1. Aerial photographs of (a) Whitehaven beach (Australia), (b) Rodds Bay (Australia), and (c) Netarts estuary (United States). The outline of these estuaries shows an irregular rather than ideal converging shape. Local confinements occur due to externally imposed restrictions, such as bedrock geology and human engineering, as well as by self-formed restrictions. The major confluences occur at locations of confinement. Google Earth, accessed January–April 2017.

forest (Townend, 2012; Figure 1). Current theoretical and empirical descriptions for estuary planforms neglect the effect that bar formation and bar evolution may have on the planform of the estuary. We propose that the irregular planform of many alluvial estuaries is shaped by a forcing mechanism in which growing midchannel bars determine bank erosion, leading to quasiperiodic widening and narrowing of the estuary.

In contrast to tidal systems, the forcing mechanism of bars has been thoroughly studied for river systems. Bars can be described as either free or forced, where forced bars are anchored to their location by the channel planform shape, while free bars can migrate freely and typically occur in straight or weakly curved channels

(e.g., Schuurman et al., 2013; Seminara, 2010; Tubino et al., 1999). For rivers, low-amplitude alternate bars may cause channel curvature, after which the alternate bars evolve into point bars, forcing a meandering planform (Schuurman et al., 2016).

A recently identified mechanism of coupling between meander and bar formation and bank erosion in rivers (e.g., Eke, 2014; Parker et al., 2011; van de Lageweg et al., 2014) may also be relevant for their tidal counterparts. In the *bank pull* condition, outer bend bank erosion causes local flow deceleration resulting in inner bend bar growth, while in *bar push* inner bend sedimentation causes transfer of flow momentum to the outer bend, which increases bank erosion. Modeling suggests that well-developed bends fluctuate around a balanced state of bar push and bank pull (Eke, 2014), but initially the alternate bars form in a straight channel (van Dijk et al., 2012) suggesting that the process of pattern formation starts with bar push. While this concept has not been applied in estuarine context, the presence of bars and bends suggests that it plays a similar role in estuarine shape and size development. Once variations in width are present, the location and size of forced bars may be induced by channel width variation, for example, due to the presence of embayments (Kleinhans & van den Berg, 2011; Leopold & Wolman, 1960; Repetto & Tubino, 2001; Schuurman et al., 2013; Seminara, 2010; Struiksma et al., 1985; Tubino et al., 1999; Wu et al., 2011; Yalin, 1971). This suggests an intimate link between bars and river planforms, and we hypothesize a similar dependency between tidal bars and estuary planforms.

Indeed, observations in modern estuaries support the hypothesis that the location where tidal bars occur correlates with by the deviation of the estuary planform from an ideal shape (Leuven, de Haas, et al., 2018; Leuven, Selakovic, & Kleinhans, 2018). In addition, bar and meander dimensions scale with estuary width (e.g., Dalrymple & Rhodes, 1995; Leuven et al., 2016; Leuven, van Maanen, et al., 2018). From aerial photographs one can observe that the locations where the estuary is relatively narrow correspond to locations with major confluences, defined as the location where two (or more) major channels connect (Figure 1). For braided rivers, the dimensions and spacing of confluences scale with bar dimensions (Ashmore, 2001; Hundey & Ashmore, 2009). Confluence locations associated to downstream bifurcations steer the morphodynamics of channels and bars (Schuurman & Kleinhans, 2015). For example, the deposition of a midchannel bar downstream of a confluence location can create a bifurcation and subsequently erode the channel banks, creating a more irregular planform (Hundey & Ashmore, 2009; Schuurman & Kleinhans, 2015). Here we explore the relation between channel and bars dynamics and estuary planform. In particular, we assess whether channel and bar dynamics can cause the often observed irregular estuary planform and the locations of major channel confluences.

Current knowledge on long-term evolution — time scales larger than decades — of bars and channels in estuaries is limited by a lack of data (de Haas et al., 2017). This is mainly due to the fact that observations in modern systems are hampered by the time scale for morphological evolution, which is much longer compared to fluvial systems. In our previous work, we studied present-day bar patterns in natural systems (Leuven, de Haas, et al., 2018; Leuven et al., 2016; Leuven, Selakovic, & Kleinhans, 2018). Here we shift focus to the morphodynamics of channels and bars. Physical scale experiments and numerical models complement observations in natural systems because they can provide higher temporal resolution, enabling detailed observation of the morphodynamic evolution of bars. In this study we use physical experiments, because the produced channel and bar patterns in numerical models (e.g., Braat et al., 2017; van der Wegen & Roelvink, 2012) depend on calibration parameters such as the transverse bed slope effect that strongly affect channel-shoal interaction and bar dynamics (Baar et al., 2018; Schuurman et al., 2018).

2. Methods and Materials

2.1. Experimental Setup and Procedure

We use a periodically tilting flume of 20 m by 3 m, called the Metronome (Figure 2), that generates dynamic tidal morphology. It produces hydrodynamic conditions capable of transporting sediment during both the ebb and flood phase (Kleinhans, Braudrick, et al., 2015; Kleinhans, van der Vegt, et al., 2017), which is uniquely different from earlier physical experiments of tidal systems that relied on periodic sea level variations (Mayor-Mora, 1977; Reynolds, 1887, 1889; Stefanon et al., 2010; Tambroni et al., 2005; Vlaswinkel & Cantelli, 2011). The downscaled magnitude of the water level variations in experiments with periodic sea level variations, while large relative to water depth, is too low to induce landward sediment transport due to the unscaled grain size. Therefore, previous experiments with periodic sea level variation resulted in systems with mainly ebb-related transport (Kleinhans et al., 2014). To obtain similar sediment mobility, scaled estuary experiments with natural sand would require a much steeper bed gradient than natural systems, because of

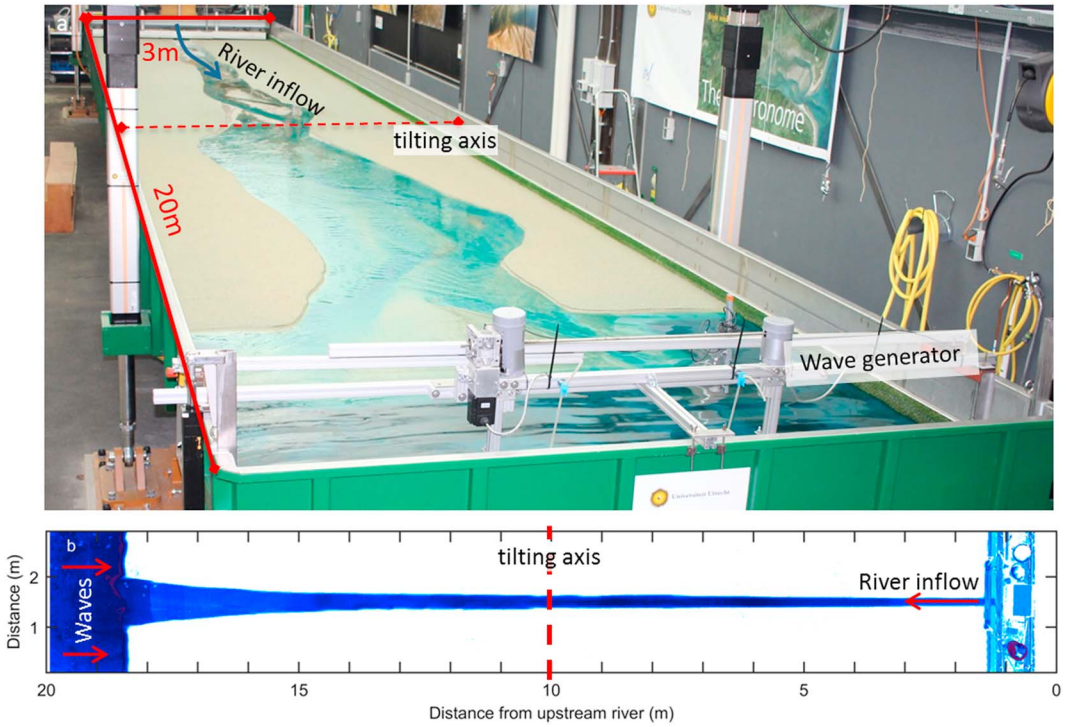

Figure 2. (a) The Metronome, a tilting flume of 20 m long by 3 m wide. (b) Overhead image of initial converging channel bathymetry. Blueness indicates depth, except in the first meter where the gantry is located. At the landward side, river discharge (0.1 L/s) was added during the ebb phase. At the seaward end, paddle-generated waves were applied during the flood phase.

their smaller water depth and bed shear stress, which we obtain by tilting the flume (Kleinhans et al., 2014, 2015). The tilting flume allows us to characterize the spatiotemporal patterns of channel and bar evolution. For a more detailed description of the design and hydrodynamics of the Metronome, see Kleinhans, van der Vegt, et al. (2017).

Here we describe one of the experiments with detailed monitoring of the bed elevation and flow velocities and study the long-term evolution of channels and bars. The experiment was run for 15,000 tidal cycles, which corresponds to approximately 20 years of natural tidal cycles assuming a semidiurnal tide. The experimental settings were selected based on a set of approximately 30 pilot experiments in which boundary conditions have been varied systematically, which are reported in the supporting information of Braat et al. (2018). The settings were selected to ensure that sediment was well above the threshold for motion and that the tidal excursion length, which is the distance a water particle travels in half a tidal cycle, was shorter than the flume length.

A plane bed of 0.07-m-thick sediment was installed on top of a mat with artificial grass in the basin. Sediment consisted of a sand mixture ($\rho_s = 2,650$ kg/m^3) with a median grain size of 0.52 mm and a coarse tail ($D_{90} =$ 1.2 mm, $D_{10} = 0.33$ mm; supporting information Figure S1). This sediment mixture was selected to prevent the occurrence of scour holes as much as possible (Kleinhans et al., 2017). Another set of experiments were conducted with the addition of crushed walnut shell to simulate the effect of cohesive material, which are reported in Braat et al. (2018). We will summarize the effect of this as far as relevant for bar growth and estuary widening in the discussion. The bed was approximately 18 m long and 3.0 m wide. An initial channel was carved in the sediment bed to facilitate the initial flow from the upstream boundary to the sea and back. This initial channel was 0.03 m deep, and the width increased exponentially from 0.2 m at the river to 1.0 m at the seaward boundary (Figure 2b).

Tidal currents were produced by four actuators that ensured a repeatable tilting with a period of 40 s and a maximum tilting gradient of 0.008 m/m. At the upstream boundary water discharge was added to the flume during the ebb phase at a constant rate of 0.1 L/s. River discharge was disabled during the flood phase, because otherwise water would pile up at the upstream boundary, resulting in an extreme water pulse when

tilted seaward again. The contribution of the river discharge to the tidal prism is 0.002 m^3 (0.1 L/s × 20 s), while the total tidal prism is about 0.11 m^3 at the start of the experiment and 0.3 m^3 at the end of the experiment (Braat et al., 2018). This means that the relative contribution of river discharge to the tidal prism is 1.8% at the start and 0.7% at the end of the experiment. This is within the range that typically occurs in estuaries, for example, between 0.01% and 20% for estuaries in the United Kingdom, with an average of 3% and a median of 0.7% (Manning, 2007).

The water level at the boundary between the sea and the land was kept at a fixed elevation by a constant head at the downstream boundary of the flume, allowing free inflow and outflow of water. Water depth in the sea was continuously compensated during the tilting by periodic vertical motion of the weir at the seaward boundary, such that the water depth in the sea was always 0.065 ± 0.005 m (Kleinhans, van der Vegt, et al., 2017). The water was dyed blue with Brilliant Blue FCF colorant to enhance the visualization of morphology.

Paddle-generated waves were introduced at the seaward boundary with a frequency of 2 Hz and an amplitude of approximately 1 cm during the flood phase. Waves were only introduced during the flood phase, because only in that phase the stirring of sand by the waves would cause slight sediment transport in landward direction. Scale effects of gravity waves in the Metronome tidal facility are described in the supporting information, but our general conclusion is that the wave-induced sediment mobility is much lower than in natural systems even though the relative wave height with respect to shoreface and channel depth is much larger. Nevertheless, waves in combination with the tidal currents were found to subdue the delta height and the tendency to form large, irregular deltas dominated by channel avulsion.

Pilot experiments showed that tilting with a simple sine function results in net exporting systems (supporting information in Braat et al., 2018), which means that the system could be classified as a delta sensu Dalrymple et al. (1992). However, we here refer to the system as an estuary, because the relative contribution of river discharge to the tidal volume is too low (≈1%) while ebb and flood currents are much larger and approximately equal (Kleinhans, van der Vegt, et al., 2017). Furthermore, the observed channels and bars in experiments resemble bars in natural estuaries (Leuven et al., 2016). Such bars are expected to form much more quickly than the time scale over which the entire estuary attains equilibrium with its forcing conditions, because bar building only requires lateral sediment displacement over short distances while estuary deformation requires displacement of sediment volumes through the entire system (Kleinhans, Braudrick, et al., 2015; Lanzoni & Seminara, 2006). We therefore argue that the main conclusions in this paper are not sensitive to this simplification.

2.2. Data Collection and Data Processing

Time lapse imagery from seven overhead cameras was collected each tidal cycle at the horizontal position of the flume when transitioning from ebb to flood flow. The cameras were mounted at equal distances 3.7 m above the centerline of the flume. The CMOS MAKO color cameras have a resolution of 2,048 by 2,048 pixels with lenses of a fixed focal length of 12.5 mm. The resulting spatial pixel resolution was 1.5–2 mm. Images were geometrically rectified, and a lens correction (vignette and distortion) was applied before they were stitched and then converted to LAB (CIELAB) colorspace images, in which *L* represents the color band with light intensity, *A* represents red to green, and *B* yellow to blue (also used in van Dijk et al., 2013). The *B*-band was extracted from the LAB images, because it enhances the visualization of morphology by the largest contrast between colored water and sediment.

The flume was illuminated at about 300 lux with daylight-colored fluorescent light aimed upward at a white diffusive ceiling at approximately 4.5 m above the flume floor. Light reflection from the water surface on the photographs was minimized by white photography backdrop cloth between the ceiling and flume.

To create digital elevation models (DEMs), photographs were taken with a digital single-lens reflex camera on a dry bed and processed with structure from motion software (Agisoft, 2017; Chandler et al., 2001; Fonstad et al., 2013; Lane et al., 1993; Morgan et al., 2017; Westoby et al., 2012). Drainage of the flume, prior to data collection, was slow enough to prevent modification of the morphology. The first five DEMs were made with an interval of 500 tidal cycles, starting at 300 cycles. Subsequently, seven DEMs were made with an interval of 1,000 cycles and the final three had an interval of 2,000 cycles. The DEMs were referenced with 20 ground control points at equal spacing on the sides of the flume, such that the resulting DEMs could be resampled on the same grid as the stitched images from the overhead cameras.

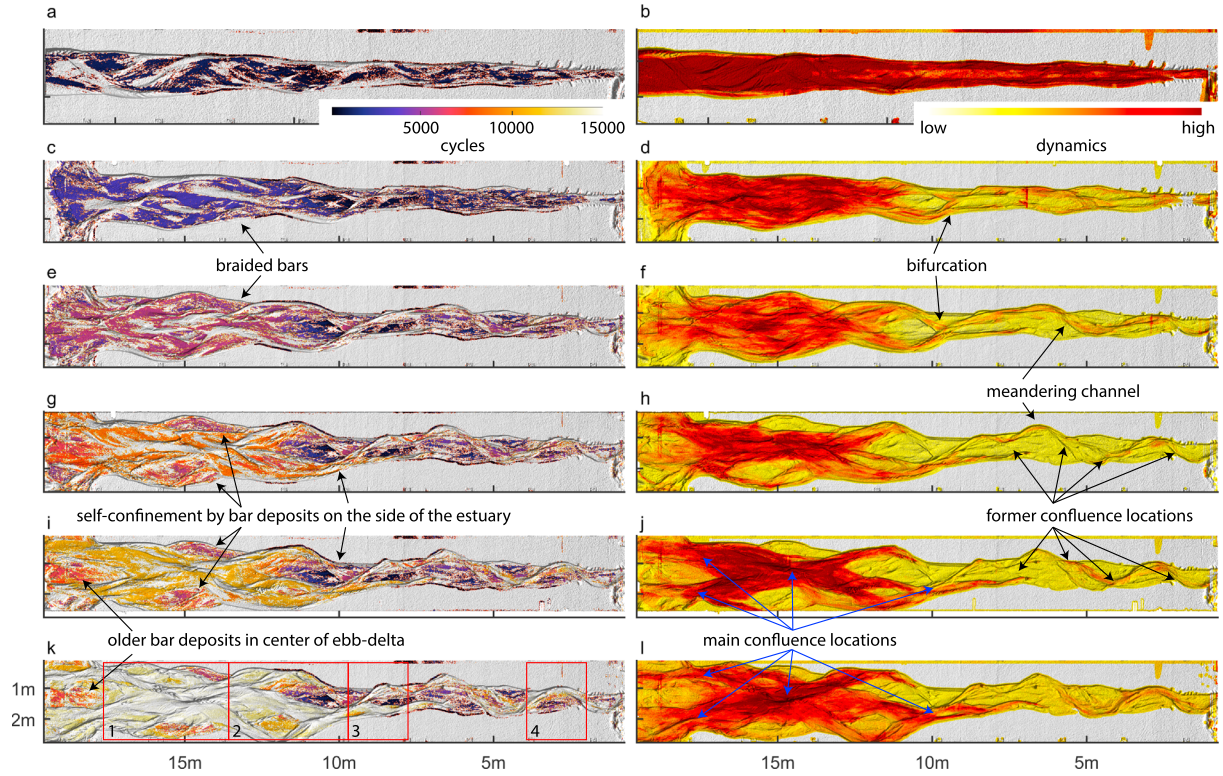

Figure 3. Two representations of spatiotemporal patterns of morphodynamics. (left column) Hillshade map of morphology at several time steps, showing increasing age variation as the system develops (top to bottom). The color scale indicates time of deposition of the top surface, where light colors are the youngest. (right column) Hillshade map of morphology at several time steps, in which the color scale indicates cumulative bed level change between two successive digital elevation models, which is an indicator of dynamic activity. Maps are given for the following time steps: (a, b) 1,250, (c, d) 3,300, (e, f) 5,900, (g, h) 8,900, (i, j) 10,900, and (k, l) 15,000 cycles. Red numbered boxes in (k) show the zones for which hypsometric curves are calculated (Figure 10c).

Flow velocities were measured over a tidal cycle with Particle Imaging Velocimetry (Mori & Chang, 2003) at 12 moments during the experiment. These 12 moments correspond with the timing of the first 12 DEMs. White floating particles (diameter ~2.5 mm) were seeded on the water surface and resupplied when necessary. At 16 equally spaced phases of the tide, 10 images were collected with the overhead cameras at 25 Hz, using a pulse train from a frequency generator. Flow velocities were subsequently calculated from pairs of consecutive images with the MPIV toolbox in Matlab (Mori & Chang, 2003). As in Kleinhans, van der Vegt, et al. (2017), we used the peak cross-correlation algorithm to determine mean particle displacement in pixels in a 50×50 window with 50% overlap. The resulting vector fields were scaled to metrics with the pixel footprint of the cameras (1.5–2 mm per pixel), correcting for the tilt of the flume. Erroneous vectors were obtained and filtered out where particles were sparse or overly abundant, as well as when the Particle Imaging Velocimetry-window partly covered the flume wall or reflection on the water surface was too large. For processing, the average vector field was calculated for each tidal phase from 10 consecutive images and for plotting purposes it was interpolated on a grid with the same size and resolution as used for the overhead cameras and DEMs. Residual currents were calculated as the average flow vector over a full tidal cycle.

2.3. Data Reduction

Experimental results are compared with data from natural systems (Leuven et al., 2016) to assess how well the tidal bars in our experiment scale to nature. A detailed comparison is made with the Western Scheldt (NL), for which detailed bathymetries over time and flow velocities are available. In this study, the important scaling properties are the planform dimensions of bars and the elevation distribution of the bathymetry. Therefore, maximum bar length and width were measured in the experiments following Leuven et al. (2016). Hypsometric curves, which are cumulative depth elevation curves, were calculated for four zones in the experiment as well as for the Western Scheldt. These zones were chosen as the part between two successive width confinements in the estuary (Figure 3k and supporting information Figure S6a).

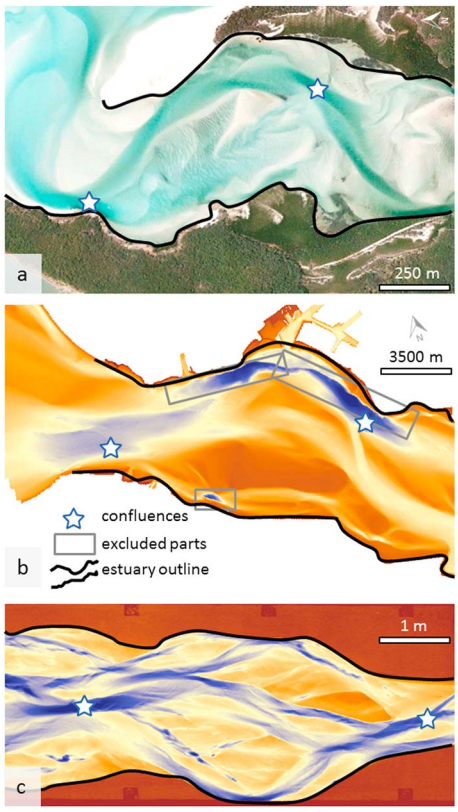

Figure 4. Locations of major confluences were determined in (a) aerial photographs of natural systems, (b) bathymetry of the Western Scheldt, and (c) experiments. Warm colors denote high elevation; cool colors denote low elevation. In case of aerial photographs, major confluence locations were chosen where multiple main channels converge. For the bathymetry of the Western Scheldt and experiment, these points were automatically determined as the maximum depth within a confluence zone. Deep scours as a result of bank protection, presence of hard layers, or outer bend erosion were excluded.

Estuary width was measured in our experiment as the local width between the noneroded estuary banks. Channel width was measured as the width of the estuary below an along-channel linear profile that was fitted on the median bed level per cross section, whereas above the median bed level was classified as bar. Excess width is defined as the estuary width minus the width from an ideal converging estuary shape and summed width of bars was measured as the sum of the width of all bars in a cross section (Leuven, de Haas, et al., 2018).

The locations of major channel confluences and the spacing between them over time were determined for the experiment and the Western Scheldt. In addition, these quantities were measured on aerial imagery for a fixed moment in time in seven other natural systems: Dovey (United Kingdom), Bannow (United Kingdom), Taw-Torridge (United Kingdom), Teign (United Kingdom), Rodds Bay (Australia), Whitehaven beach (Australia), and Netarts (United States). In case of aerial photographs, major confluence locations were visually determined as the deepest point where multiple channels converge, while these points were extracted from bathymetric data for the experiments and Western Scheldt (Figure 4). Deep scours as a result of bank protection, resistant layers that consist of shell fragments (so called *crags*; Cleveringa, 2013), or scours associated with outer bends of meanders were excluded. Subsequently, the location and spacing between successive channel confluences were measured with respect to local zones of confinement in the estuary outlines.

The dynamics of channels and bars over time were studied from the blueness images, which is a proxy for the water depth. Blue represents the channel and white the bar. Changes in blueness values were used to study where erosion and sedimentation occurred in the experiment and to determine the youngest time step during which sediment was deposited. The same approach was applied using successive DEMs of the experiment, but the temporal resolution for this was lower. Cumulative bed level change was calculated as a measure of the spatial dynamics within the system and to assess whether the experiment was in dynamic

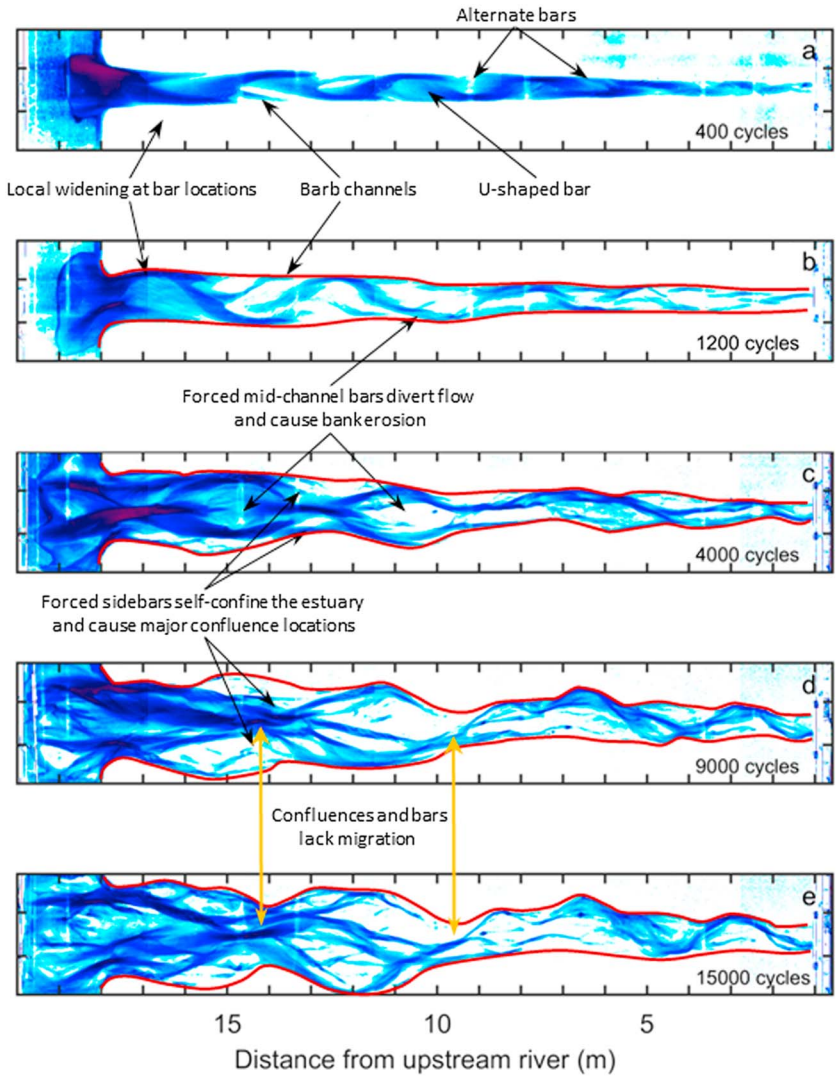

Figure 5. Overhead imagery of the experiment for (a–e) five moments in time. Blueness was extracted as an indicator for channel depth. For an overview of all time steps, see supporting information Figure S2 or the supporting information Movie S1.

equilibrium during the final stages. Cross-sectional profiles were taken from the LAB images and plotted over time, creating time stack diagrams that show the migration of channels and bars in cross section over time.

3. Results

3.1. General Morphological Evolution

In the initial phase of the experiment, an alternate bar pattern evolved (Figure 5a). As channel widening continued, a main meandering channel formed with riffles between two successive bends. The meandering channel and alternate bars initially migrated seaward (supporting information Movie S1). Later, the increased curvature of the meandering channel forced the bars to become anchored to their inner bends, while lateral erosion and deposition increased the width of the forced bars. In a later stage, channels stabilized in the landward part of the estuary, while the estuary width kept increasing in the seaward part. This allowed the development of multiple bars and channels in cross section, which were first observed when flood *barbs* intersected the forced bars (Figures 5a and 5b). Barb channels are channels that become shallower in the direction of flow and have a dead end on the bar. Net sediment transport toward the sea formed an ebb tidal delta, which is a term more commonly used in the context of tidal basins and also applies to estuaries (e.g., Davis & Hayes, 1984; Elias et al., 2017). The ebb tidal delta limited the inflow of water to the estuary. As widening progressed, forced midchannel bars diverted the flow and periodically caused bank erosion. These zones were

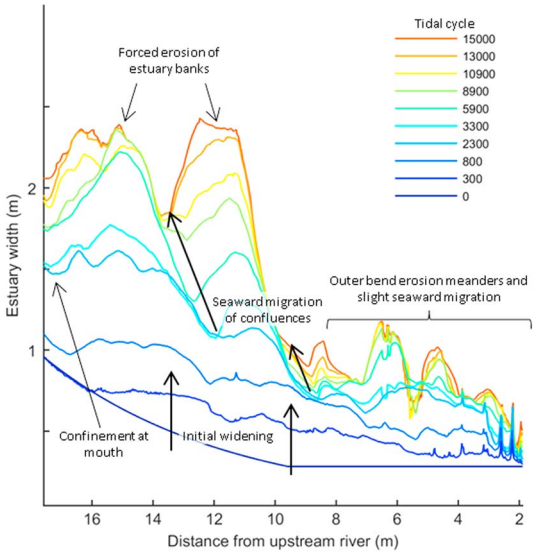

Figure 6. Evolution of the estuary width profile. The planform initially widened and, from 2,300 cycles onward, became more irregular. After 3,300 cycles, bars and landward meanders rapidly force local widening, while confinements migrate seaward. In the last phase, after 8,900 cycles, the bars became static (forced) and bank erosion ceased at the confluence locations, while the amplitude of the quasiperiodic width variation increased where midchannel bars were present.

alternated by locations where the estuary width remained narrow or was self-confined by sidebar deposits, resulting in a quasiperiodic planform (Figures 5d and 5e).

3.2. Channel Widening and Incipient Meandering

The initial phase of the experiment was characterized by the development of the initial converging channel into an incipient meandering ebb tidal channel (Figure 5a). In the first 200 cycles, the converging straight channel widened (Figure 6) and initially free (seaward migrating) alternate bars formed. The resulting channel pattern consisted of multiple straight channels parallel to the centerline of the estuary, which were separated by sills that connected the alternate bars in along-channel direction. Over time, the straight channels became more oblique to the estuary centerline and curved until they developed a meandering ebb tidal channel, which forced the bars in place. On top of the alternate bars, circulating flow patterns developed, with residual currents dominantly moving in landward direction onto the bars, then diverting to the channel and flowing back in seaward direction via the meandering channel (Figure 7a). Both the ebb and flood flows caused erosion of the estuary banks by lateral migration of channels in the following tidal cycles (Figure 7b).

3.3. Alternate Bars With Initial Barb Formation

This phase was characterized by the formation of barb channels in the inner bends of the alternate bars. The main meandering ebb channel migrated laterally eroding the estuary banks, and alternate bars grew in width. At the landward side shallow sills formed between two successive alternate bars. The sill separated the ebb flow from the flood flow in two separate channels. As the ebb channel migrated further seaward and the flood channel landward, u-shaped bars formed (Figure 5a). The u-shaped bars thereby partly blocked the channel with opposing flow (Figure 5a).

From 1,000 tidal cycles onward the braiding index, which is the average number of channels or bars in the cross section, kept increasing as a result of the increasing channel width, which allowed for multiple braided bars (Figure 5a). Bars were particularly abundant in specific zones (at approximately 8, 11, 14, and 15 m) where the summed width of bars was large (Figures 8a and 8b) and the compound bars were dissected by one or multiple barb channels. Compound bars are more complex bars that probably amalgamated from other bars, in analogy with rivers (e.g., Ashworth et al., 2000; Bridge, 2003; Schuurman et al., 2013).

At the seaward side, the export of sediment during the first 2,000 cycles formed an ebb tidal delta. After this period, the delta was large enough to limit the inflow of water into the estuary, while erosion on the delta formed a single major channel at the northern side of the inlet (supporting information Figures S2h and S2i).

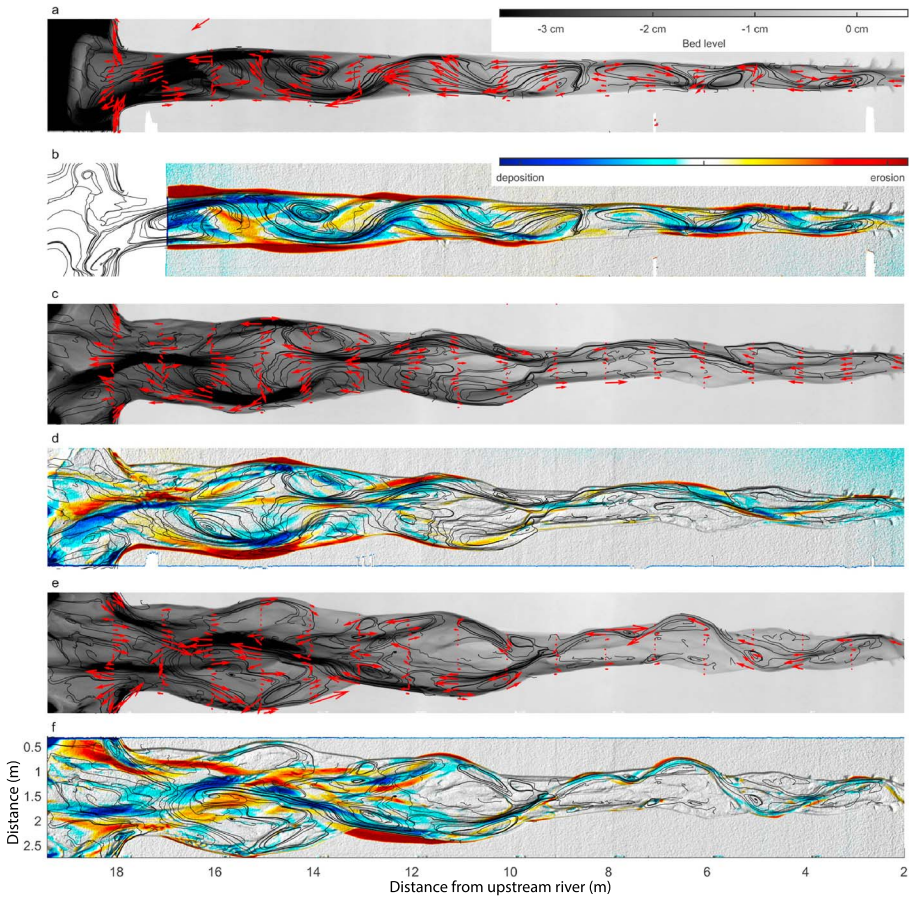

Figure 7. (a, c, e) Vectors indicating the residual currents after (a) 800, (c) 4,400, and (e) 6,900 cycles for transects with a spacing of a meter on top of a map with the streamlines based on a vector field with residual currents and the bathymetry. (b, d, f) Streamlines based on a vector field with residual currents, plotted on top of a map that indicates the erosion (in increasing magnitude from yellow to red) and sedimentation (from cyan to blue) in the subsequent phase of the experiment.

The location of the main meandering channel shifted from north at 1,000 cycles to south around 2,000 cycles and back north at about 3,000 cycles at approximately 15 m from the upstream boundary (supporting information Figures S2e, S2h, and S2i). Interestingly, the adjacent channel confluence positions (at 13.5 m and at the mouth of the estuary) were relative stable over time, with dynamic bar and channel zones in between. This caused a rather irregular pattern in the outline of the estuary where some parts remained relatively narrow, while other parts became relatively wide (Figure 6).

3.4. Midchannel Bars, Confluences, and Evolution of Quasiperiodic Planform

In the central part of the estuary (8–18 m), widening resulted in the formation of forced midchannel bars that diverted flow, which caused bank erosion. For example, after 4,000 cycles, a large estuary width at 15 m allowed the existence of two major channels: one on the northern side and one on the southern side of the estuary, separated by a relatively wide bar in the center of the estuary (Figure 5c). The confluences of these two channels occurred at the mouth of the estuary and at 13.5 m in a channel located in the middle of the estuary. While the two major channels at 15 m continued to migrate toward the outer banks of the estuary (Figure 9d), the bar between these channels obtained an oval shape as a result of an almost symmetrical ebb and flood barb on both its landward and seaward side. The residual current showed two major circulation cells at this compound bar (Figure 7c). The flood barb facilitated flow onto the bar, which diverged over the bar to the channels north and south of the bar. The ebb flow predominantly used the northern and southern channels around the bar, and any flow entering the ebb barb also diverged into these channels. This caused bank erosion on both the north and south sides of the estuary and sedimentation that increased the width

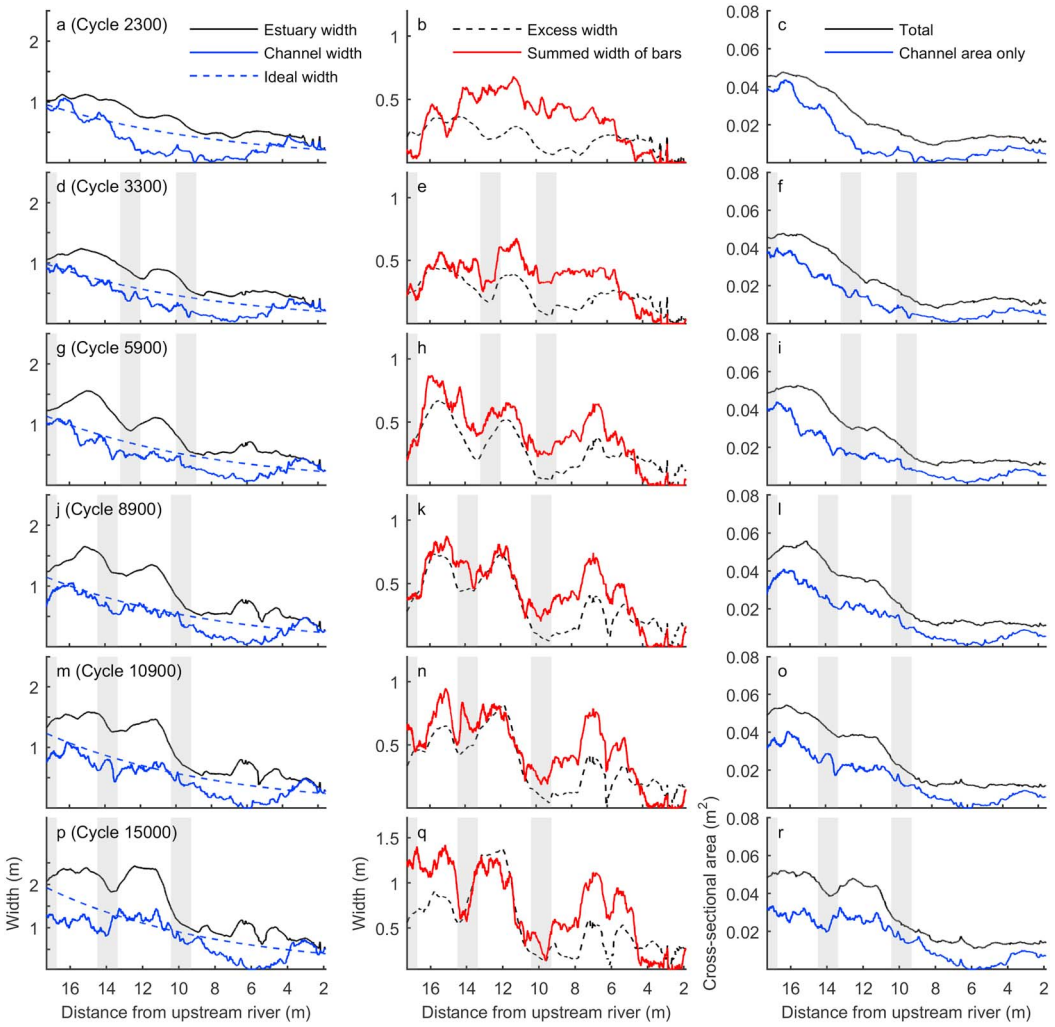

Figure 8. (a, d, g, j, m, p) Evolution of estuary width, channel width, and ideal width. (b, e, h, k, n, q) Evolution of excess width and summed width of bars. (c, f, i, l, o, r) Evolution of cross-sectional area. Estuary width is the sum of channel and bar width. Ideal width is the largest fitting exponential shape in the estuary outline. Excess width is the estuary width minus the ideal width. The channel width approaches an ideal converging shape over time. Summed width of bars approaches the excess width. Total cross-sectional area is the area below the estuary banks. Channel cross-sectional area excludes the area above bars. Shading indicates the locations where the estuary remained confined. At these locations, the summed channel width and summed bar width remain relatively low.

of the midchannel bar (Figure 7d). A similar process occurred in a more landward part slightly later in the experiment.

In the landward part of the estuary (0–8 m) the individual channels became more curved and connected, so that a main meandering channel formed from 5,000 cycles onward (Figures 5c and 5d). The channel orientation of the upstream channel affected diversion of flow and sediment at the former bifurcation at 9 m, so that now the landward river system fed the southern branch instead of the northern branch (Figures 5c and 5d). This channel subsequently migrated (Figure 9c) by eroding the southern bank of the estuary at 10 m (Figure 7f), whereas the northern channel was only connected during flood flow. Seaward, the southern channel merged with the major channel that formed in the middle of the estuary at approximately 13 m. At this point multiple smaller barb channels formed onto the bar at 11 m that evaded each other and migrated over the bar.

At the mouth, the estuary was slightly narrower than the part of the estuary directly landward of the mouth at 16 m. Specific zones occurred where estuary width was relatively narrow with a major confluence and approached its ideal width. The zones were alternated by zones in which the estuary was much wider

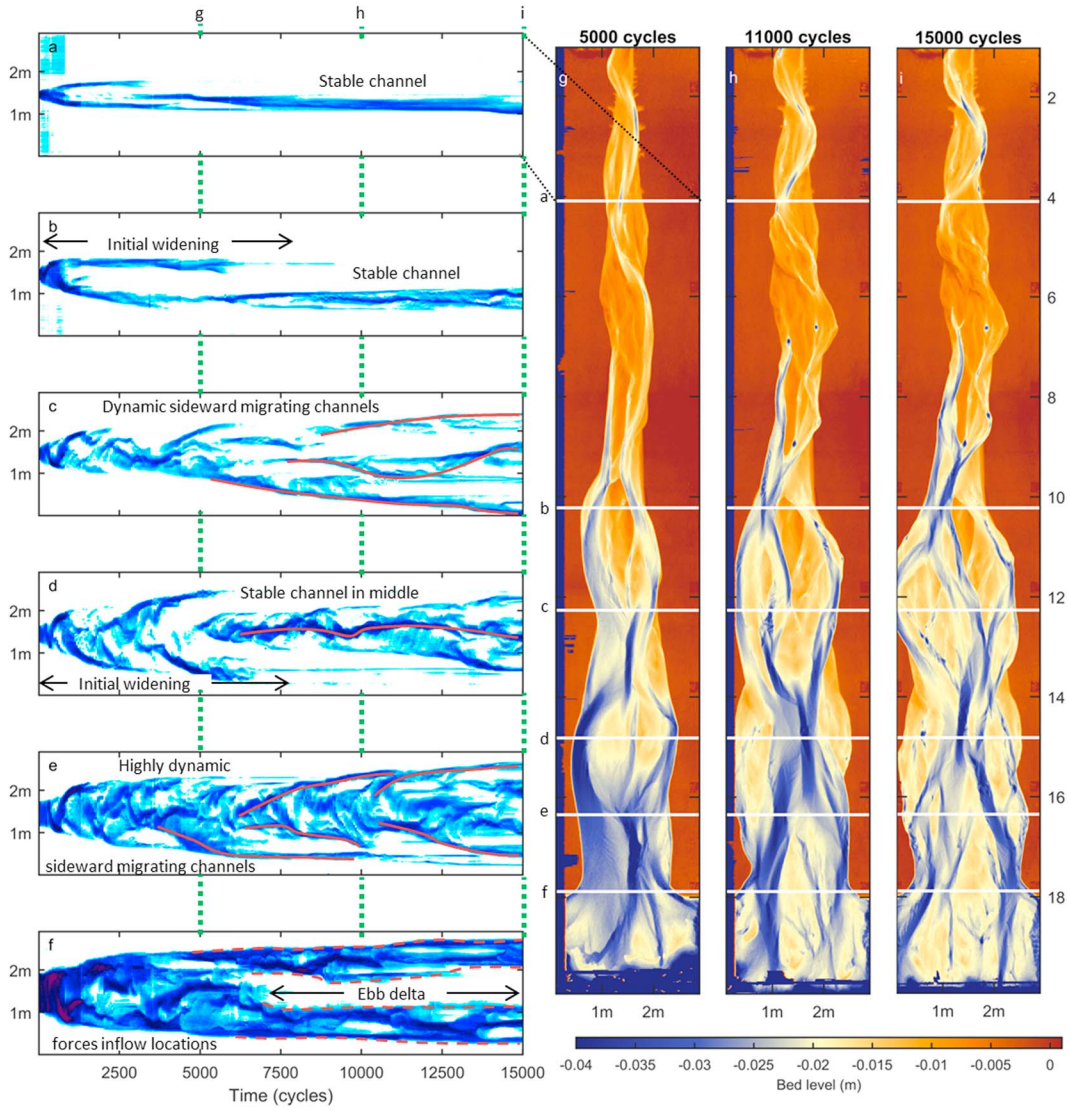

Figure 9. (a–f) Time-space diagrams of cross sections at 4, 10, 12, 14.5, 16, and 17.5 m, which are indicated in (g, h, i) bathymetry after 5,000, 11,000, and 15,000 tidal cycles. (a, b) A single landward channel stabilizes from 7,500 tidal cycles onward. (c) In the center, dynamic, sideward migrating channels occur. (d) Outward migrating channels erode the estuary banks. From about 6,000 cycles the midchannel bar is crosscut and a single main channel forms in the middle of the estuary. (e) In the seaward part, multiple very dynamic, migrating channels occur. The channels migrate from the estuary centerline toward the estuary banks. (f) An ebb tidal delta forms and stabilizes after 7,500 tidal cycles. This diverts the inflow locations to be on the sides of the ebb tidal delta.

(Figure 8). Over time, the confluences migrated slightly seaward and the planform became progressively less ideal (Figure 6). The landward channel (0–8 m) eroded the estuary banks in the outer bends of the meanders until approximately 8,000 tidal cycles. From that moment on the configuration of channels and bars in the landward part (0–8 m) remained relatively stable over time (Figures 5d, 5e, 9a and 9b). The later phases of the experiment (6,000–15,000 cycles) were characterized by specific zones that were active (Figures 3h, 3j, and 3l). These zones connected the major channel confluences at 10, 14, and 18 m. The active zones were relatively narrow at locations where the confluences occurred (e.g., at 14 and 18 m in Figure 3j) and relatively wide in the zones in between (e.g., at 16 m).

3.5. Crosscutting of Midchannel Bars

In the seaward part, the phase with midchannel bars and bank erosion continued until 5,000 cycles, when a channel was able to progressively cut through the middle of the bar, connecting the barb channels around 5,000–5,500 cycles (Figures 5c and 5d). This caused a main channel along the centerline of the estuary.

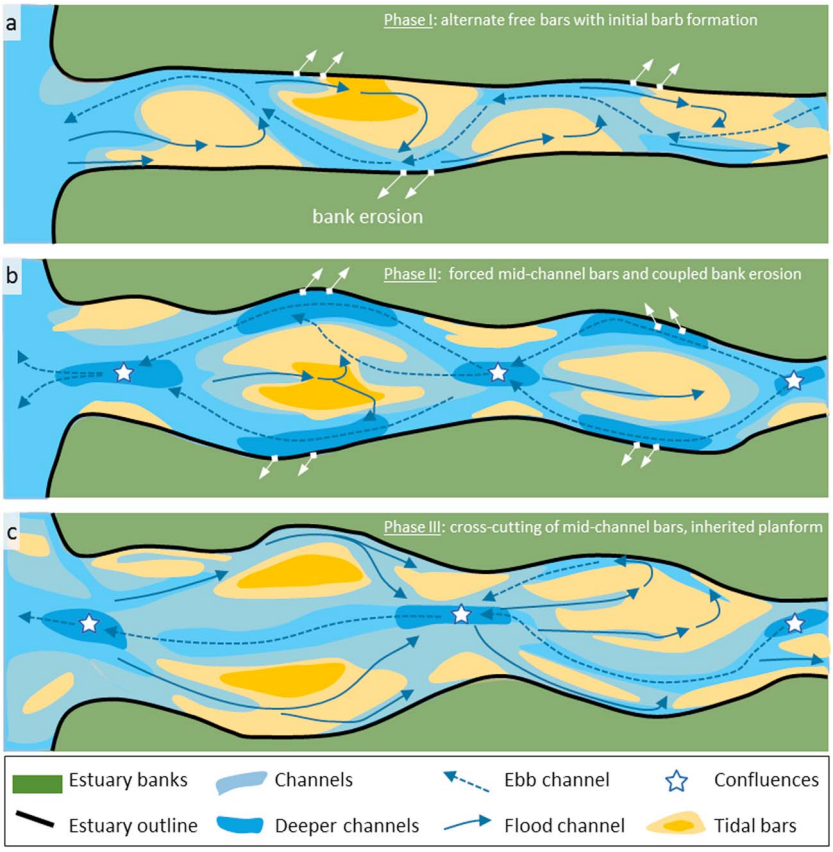

Figure 10. Conceptual model for the development of self-formed estuaries. (a) Phase I: the initial converging channel widens and (free) migrating alternate bars form. The meandering channel around the alternate bars is predominantly used as ebb channel, eroding the outer bends. While the alternate bars widen, initial flood barbs form onto the alternate bars. The main meandering channel migrates slightly seaward in Phase I, causing a longitudinal displacement in the next phase. (b) Phase II: the flood barb channels progressively cut through the alternate bars, isolating forced midchannel bars in the middle of the estuary. This creates two major confluences: one at the mouth and one upstream of the midchannel bar. The flow is diverted around the midchannel bar, which causes bank erosion, resulting in an even more irregular planform. (c) Phase III: the barb channels on the midchannel bar enlarge and subsequently connect, crosscutting the bar. This forms a new channel in the middle of the estuary and limits the erosion of the estuary banks. The resulting quasiperiodic planform is inherited from phase II. Major confluences separate zones in which channels periodically rework tidal bars.

During this phase, the major inflow and outflow were focused in the middle of the ebb tidal delta. This reduced bank erosion in the most downstream part of the estuary from that moment onward (Figure 6; 14–18 m), preventing the estuary shape from becoming more irregular.

In the central part of the estuary, the crosscutting event also caused the direction of the residual circulation cells to reverse, with flood flows now predominantly occurring along the sides of the estuary, while the channel in the middle of the estuary was ebb dominant (Figure 7e). This reduced erosion of the estuary banks at this location and triggered the formation of new channels that connected the main ebb channel with the newly formed outflow locations on the ebb tidal delta (Figure 7f). Because the main channels in the middle of the seaward part of the estuary (14–18 m) gradually exported sediment to the central parts of the ebb tidal delta, this process eventually blocked the inflow and outflow of water (6,000–8,000 cycles; supporting information Figure S2n–S2p). The ebb delta thus stabilized in place after 7,500 tidal cycles (Figures 9f and 9h), after which the inflow and outflow of water became diverted to the northern and southern sides of the ebb tidal delta (Figure 9f).

Similar to the previous bar crosscutting event around 5,000 cycles, a similar process occurred at the compound bar more landward (9.5–13 m), where after 9,000 cycles the crosscutting of the middle parts of the bar occurred (Figure 5d). This isolated a southern part of the compound bar at 9.5 m. In short, the estuary evolved

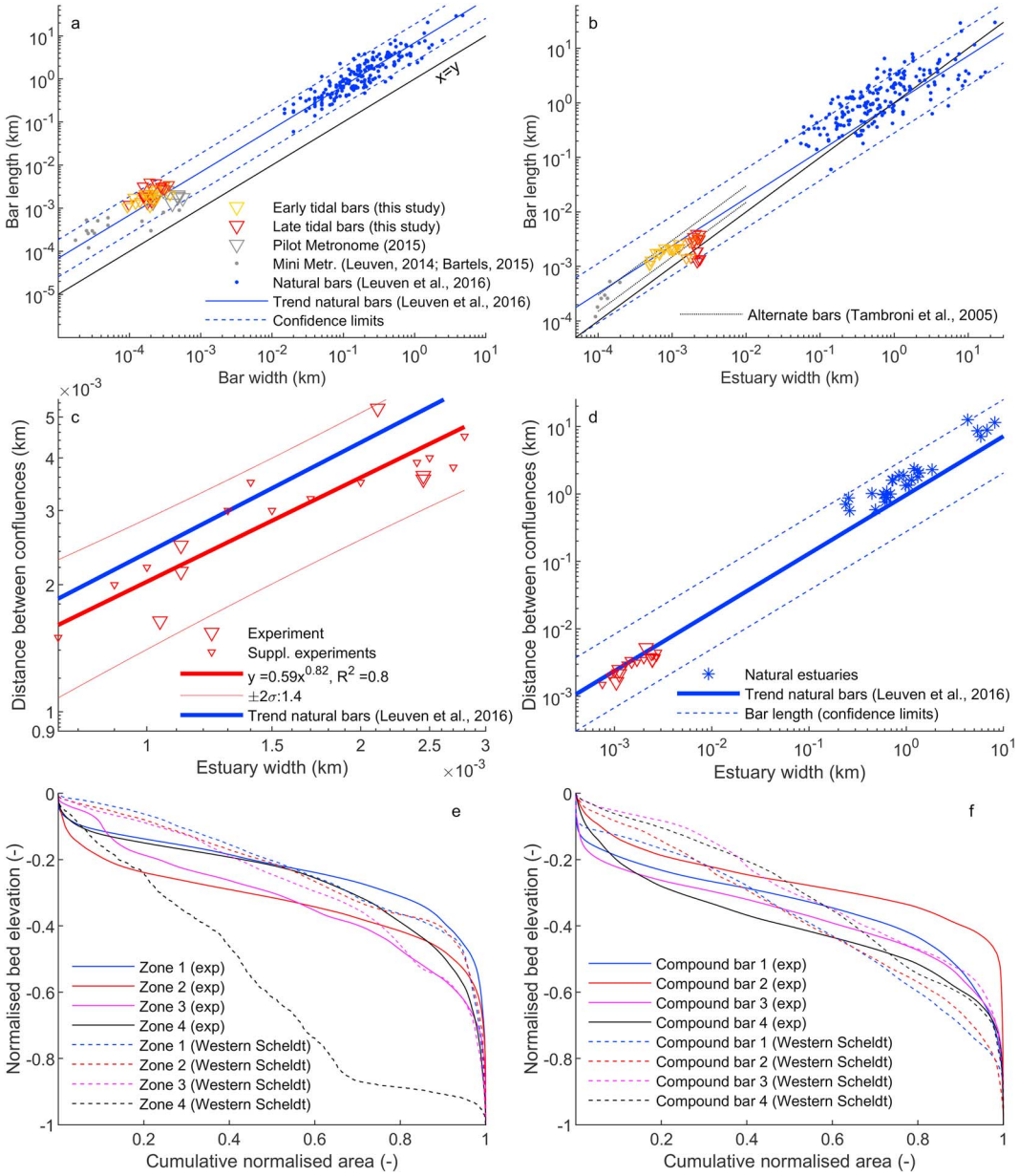

Figure 11. (a) Comparison of planform bar dimensions (length versus width) in the experiments and in natural systems. Triangles represent bars in the experiment, with color indicating the tidal cycle during which the bars were measured: yellow was early in the experiment; red was at the end. (b) The scaling relation between estuary width and bar length that was found for natural systems holds for the experiments (Bartels, 2015; Leuven, 2014; Tambroni et al., 2005). (c) Confluence spacing as a function of local estuary width for experiments. Each triangle is the spacing between two successive confluence locations. (d) Comparison of confluence spacing in experiments with natural systems. A line with predicted bar length (×1.5) is drawn for comparison and shows that confluence spacing scales with bar dimensions and estuary width. (e) Hypsometric curves of zones between two successive confinements in the estuary outline, with numbering increasing in landward direction. The corresponding zones are given for the experiment in Figure 3k and for the Western Scheldt in supporting information Figure S6a. Parts above the high water level were excluded. (f) Hypsometric curves of compound bars in the same zones.

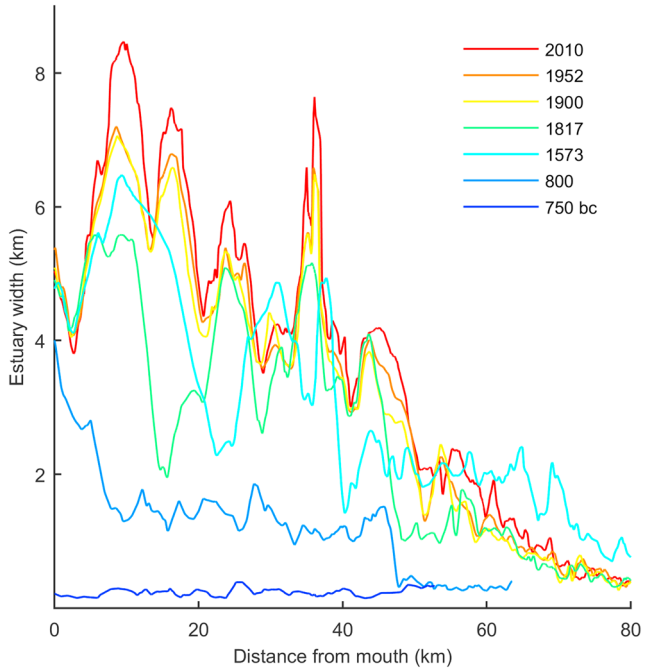

Figure 12. The estuary width profile of the Western Scheldt (Netherlands) over time, which shows a similar evolution as the experiment.

from an initially converging channel into an estuary filled with bars that inherited its quasiperiodic planform from phases in which midchannel bars diverted flow laterally, causing bank erosion.

3.6. Progressive Infill From the Sea and Dynamic Equilibrium With Stable Confluences

The zones where the estuary was confined reflect the locations where bars were relatively less abundant. For natural systems, a correlation was found between the occurrence of tidal bars and locations where the excess width is large (Leuven, de Haas, et al., 2018), which is defined as the local estuary width minus the ideal estuary width. This is in agreement with the experimental results (Figures 8h, 8k, and 8n), where summed width of bars indeed approaches the excess width in the later stages of the experiment. While the zones between 4–8 m and 14–18 m deviated from this rule in magnitude, the along-channel pattern is the same, that is, low excess width corresponds to low summed width of bars and vice versa.

In the last phase, the estuary reached a dynamic equilibrium with stable confluences, while active channel migration remained in the parts between the confluences. Mean changes in bed level and sediment export illustrate that the experiment was close to dynamic equilibrium (supporting information Figure S3). Generally, the increase in estuary width that was observed in previous stages decreased and only in the part 10–13 m and at the mouth of the estuary a slight increase in width occurred during the last 2,000 cycles of the experiment (Figure 6).

In the final stages of the experiment, flow from the landward side bifurcated around the newly isolated bar at 11 m (10,000–12,000 cycles; Figures 5d and 5e), after which the northern branch began to erode the southern side of the former bar between 9.5 and 12 m. At the same time the southern branch continued to erode the southern bank of the estuary until reaching the flume wall, which was the reason to end the experiment after 15,000 cycles.

4. Discussion

This study presents the first physical scale experiment of an estuary with dynamic channels and bars, stable confluences, and a self-formed planform. Below, we first describe a conceptual model on how forced bars determine the estuary outline. Second, we discuss the spatial and temporal scaling of bars. Then, the effect of bar patterns on the flow patterns is compared with the evolution of natural estuaries. Last, the observed experimental cyclicity in channel and bar migration is compared to natural systems.

4.1. Conceptual Model for Estuary Planform Forcing

We summarize the evolution of a self-formed estuary in a conceptual model containing three phases. In the first phase (Figure 10a) an alternate bar pattern develops, while the estuary widens. The initially straight channels connect to form a meandering channel with alternate bars (comparable to alternate bars in rivers Ikeda & Parker, 1989; Struiksma et al., 1985; van de Lageweg et al., 2014). As soon as the bars exceed a width-to-length ratio of approximately 1/7, the flood flow is capable of forming barb channels onto the alternate bars (Figure 13a). The barb channels progressively cut through the alternate bars. Both the outer bends of the meandering channels and the flood barbs erode the estuary banks, which creates an irregular estuary planform.

In the second phase, the first mid-channel bars have formed that are large enough to divert the flow such that the outer bend erosion is accelerated and major confluences are formed seaward and landward of the mid-channel bars forming a quasi-periodic estuary planform (Figure 13b). At the confluence locations, estuary width generally remains narrow and dynamic channels and bars only occur within a small stretch of the estuary width. As outer bend erosion continues, the gradient over the midchannel bar becomes favorable for both the ebb and the flood flows. These flows create new barb channels onto the midchannel bar, which over time are capable of crosscutting the bar, forming a new main channel in the middle of the estuary (Phase III;

Figure 13c). The timing of this event may vary along the estuary, and confluences typically migrate seaward over the course of these phases.

After this phase, a dynamic equilibrium at the bar confluence scale is reached, in which sediment from bars and banks is reworked into new bars within the estuary. The confluences remain stable, and bank erosion is reduced. Dynamic zones of channels and bars typically occur in stretches between the major confluences. In both experiments and natural systems we observed the development of irregular estuary planforms and the forcing of channel confluences and zones with dynamic channels and bars. The conceptual model implies that quasiperiodic deviations from the ideal estuary shape can be formed autogenically. This means that the planform shape of natural estuaries is not necessarily externally forced, that is, allogenic, for example, by the presence of bedrock or resistant layers.

Our observations show that the mechanisms of bar push and bank pull identified in rivers (e.g., Eke, 2014; Parker et al., 2011; van de Lageweg et al., 2014) may apply in estuaries as well. Initially, the alternate bars form in a straight channel, which was also the case in river experiments (van Dijk et al., 2012), suggesting that the process of pattern formation starts with bar push. However, in later phases, as soon as the increased curvature and local widening (e.g., Repetto & Tubino, 2001; Seminara, 2010; Zolezzi et al., 2012) forces the bars to be nonmigratory, the usual meander bend migration mechanism of curvature-driven momentum displacement toward the outer bank kicks in, causing bank retreat. This is followed by inner bend accretion, meaning that this phase is dominated by bank pull. Upon further widening, the bar regime shifts to midchannel bars that are nonmigratory because of curvature and local widening as well as the tidal reversing flow, and the process continues on both sides of the bar. We hypothesize that this stage is dominated by a balance between bank pull and bar push as in Eke (2014).

4.2. Spatial and Temporal Scales of Channels and Bars

The dimensions of tidal bars in the experiments scale well with bars observed in natural systems, as reported in (Leuven et al., 2016; Figure 11a). All experimental bars are within the uncertainty margins given for natural bars. However, most experimental bars plot above the trend line, indicating that their shape is slightly more elongated compared to the bars in natural systems (length-to-width ratio of approximately 8 in experiments, compared to 7 in nature). Moreover, the bar length is well within the range as expected based on local estuary width (Figure 10b). The experimental bars have similar dimensions as the alternate bar pattern reported in Tambroni et al. (2005) where the average bar wavelength is 3–6 times channel width; thus, bar length is 1.5–3 times channel width. However, in contrast with experiments with fixed channel planimetry (Tambroni et al., 2005, 2017) that result in a system with a braiding index of 1, we observed rapid widening of the estuary, which allows braiding index, bar width, and bar length to increase. Most experimental bars fall exactly on the trend expected from natural systems. The largest outliers occur at the lower uncertainty band. These bars are an order of magnitude smaller than the other bars and formed in later phases of the experiment in one of the larger channel branches in the estuary. In this case, the width of the single branch is responsible for the bar dimensions. Therefore, scaling with the full estuary width may result in large deviations from the expected trend.

Hypsometric curves for four zones within the estuary (indicated in Figure 3k and supporting information Figure S6a) show a large similarity between the experiment and the Western Scheldt (Figure 10e), where zones were defined as the estuary area between two successive confinements. Only zone 4 in the Western Scheldt deviates significantly from the hypsometry in the experiment (Figure 10e). At this location the estuary width is smaller and thus a larger part of the width is influenced by dredging to maintain shipping fairways. When channels are excluded and thus hypsometric curves are drawn for compound bars only, bars in the Western Scheldt show a more linear elevation profile, while bars in the experiment have a more s-shaped curve (Figure 10f). The s-shaped curves for the experiment are caused by a small portion of the compound bars being highly elevated and a small portion being very low elevated. High elevated parts developed on the oldest parts of bars that accreted over time and lack flooding and morphodynamic activity in later phases. The relative scarcity of high elevated areas is caused by the lack of cohesive material and vegetation, which would otherwise accrete tidal bars and estuary banks (Braat et al., 2018, 2017; Lokhorst et al., 2018). Low elevated parts are previous channels or scours on bars for which time was too short to fill in.

As bars separate the major confluences, it was expected that confluence spacing scales with bar dimensions, which scale with estuary width (bar length $\propto$ channel width$^{0.87}$; Leuven et al., 2016). Indeed, this was found to be the case (Figures 10c and 10d), which means that the spacing of confluences scales well with

bar dimensions and estuary width. In general, this also implies a decreasing confluence spacing along channel from the sea in landward direction, because estuary width and bar dimensions decrease. To quantify the location where confluences occur, we measured the distance from the location of the major confluences to the local minima in the outline of the estuary. The measured distance was normalized by the average spacing with the successive landward and seaward confluence locations. Results show that the major confluences in all cases occur within 16% of local confinements for the experiments and Western Scheldt over time, as well as for the aerial photographs of eight natural systems (supporting information Figure S4).

The time scale over which the channels and bars in the experiment evolve is 15,000 tidal cycles, which corresponds to approximately 20 years of natural tidal cycles. All the sediment eroded in the experiment is either used for bar formation or exported to the ebb delta, which is a long-term sink for the eroded sediment because of the lack of intense littoral processes. Most modern estuaries typically evolved over centuries to millennia during the middle to late Holocene under rising sea level (de Haas et al., 2017; Hijma & Cohen, 2011; van der Spek & Beets, 1992). As such, their evolution comprised many more tidal cycles than our experimental estuary. Typically, modern estuaries initially enlarged as former river valleys that drowned, because of the rapid sea level rise around the start of the middle Holocene. Part of the slower evolution may thus be explained by the time required for aggrading after sea level rise decreased, in contrast to the erosional behavior in the experiment. The relatively rapid evolution of bar patterns and bank erosion was also observed in river experiments and may partly be explained by a lack of bank strength in experiments without vegetation and cohesive material (van Dijk et al., 2012).

Additional experiments with added cohesive material (Braat et al., 2018) revealed two major effects compared to the experiment reported in this study. First, the mud fills up inactive areas and predominantly accretes on the tidal bars and estuary banks, which reduced the tidal prism. This counteracts the positive feedback mechanism between estuary widening, increased tidal prism, and therefore increased cross-sectional area at the mouth. The second effect is that the cohesiveness of mud has a slight stabilizing effect on gentle slopes. However, the cohesion has no effect on the bank erosion rate as bespoke experiments demonstrate. The combined effects result in a narrower, confined estuary planform, but with similar bar patterns and dynamics, although higher in elevation, compared to the experiment without cohesive material reported here (Braat et al., 2018).

Nevertheless, the general evolution of the experiment can be compared to the Western Scheldt, which evolved in the past 2,700 years from a narrow creek in a peat bog to an alluvial estuary with a quasiperiodic planform (Figure 12). The time scale over which estuaries widen from a narrow creek after ingressions is typically in the order of hundreds of years, which may still be an estimate on the higher end for organic peat, which decays rapidly after erosion (de Haas et al., 2017; Pierik et al., 2017) and thus does not contribute to sediment available for bar formation. Despite their contrasting early evolution, the later stages of the experiment and natural systems were more similar.

Bar dynamics typically occurs in tidal inlets, embayments, and estuaries on time scales from 15 to 40 years (Israel & Dunsbergen, 1999; Levoy et al., 2017). A comparison of the experiment with this time scale may be more appropriate, because these processes are not limited in sediment supply. Nevertheless, scaling relations for bar patterns in experiments (Kleinhans et al., 2015) and the natural processes that form bars (Leuven et al., 2016) and confine estuaries are not well understood. Recent numerical models show that mud deposits may be required to confine estuary planform and that self-formed estuaries with mud can reach an equilibrium within 500–1,000 years (Braat et al., 2017).

4.3. Role of Circulation Cells and Confluences on the Evolution of Estuaries

The historic evolution of channel and bar patterns in the Western Scheldt (1800–1900) was characterized by an initial phase of migration and meandering of the main ebb channels, after which the meander bends reached the embankments on the sides (Jeuken, 2000). In the inner bends, the compound bars extended laterally and flood barbs formed. This evolution is very similar to the initial phases of the experiment (Figures 6 and 11). However, after 1900, the morphological evolution was largely influenced by human interference: dikes were constructed, side branches that slowly filled-in were embanked, and the first dredging activities started in 1922 (Jeuken, 2000; Kleinjan, 1938).

In 1944, van Veen (1944) described the occurrence of circulation patterns in the Western Scheldt, where flow circulates through an ebb and a flood channel enclosing an intertidal bar. These circulation cells are similar to

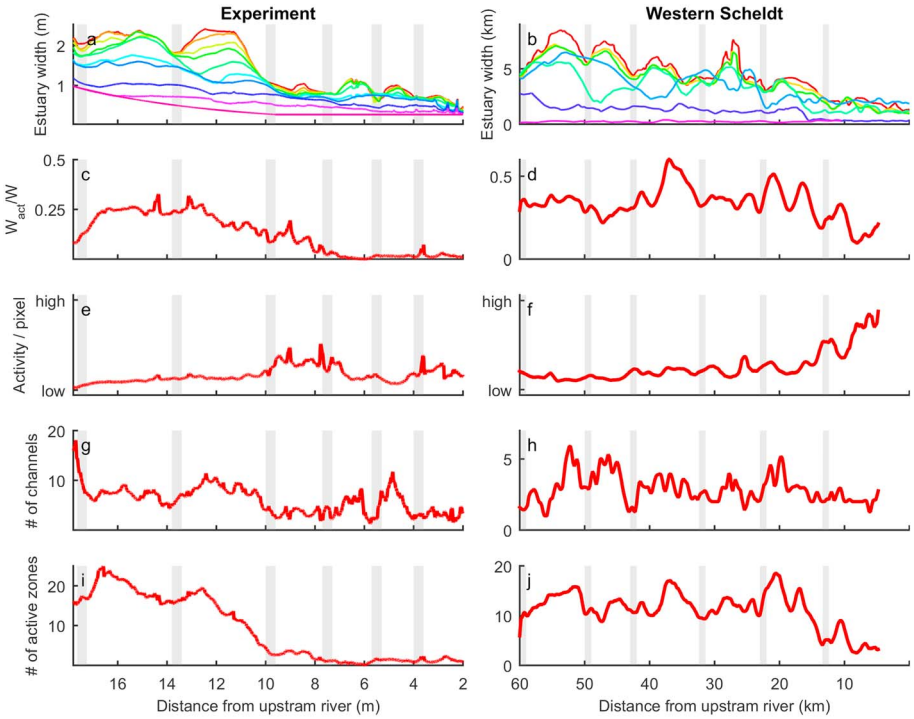

Figure 13. Along-channel profiles of (a, b) local estuary width over time, (c, d) time-averaged active channel width normalized with local estuary width, (e, f) sum of absolute bed level change per pixel, (g, h) number of channels in cross section, and (i, j) number of active areas in cross section. Shading indicates locations of confinement in the estuary outline. These locations correspond with locations where the active width, activity per pixel, and number of channels are generally low. The along-channel profiles (c–j) were averaged over the period 7,500–15,000 cycles for the experiment and the years 2000–2015 for the Western Scheldt.

the circulation cells observed in the experiment, where the main meandering channel is ebb dominated and circulation cells covered the flood barb and adjacent ebb channel. These circulation cells divide the Western Scheldt into six main zones, which were later described as macrocells (Jeuken & Wang, 2010; Monge-Ganuzas et al., 2013; Toffolon & Crosato, 2007; Winterwerp et al., 2001); supporting information Figure S6). These cells were determined from the observed morphology of the main ebb and flood tidal channels and numerically modeled residual flow, which resulted in cells that covered the enclosed area of an intertidal compound bar with its surrounding meandering channel. The boundaries of these cells in along-channel direction were chosen at the location of major channel confluences and correspond to the locations where the estuary width is relatively narrow. The concept of macrocells (e.g., Jeuken & Wang, 2010; Monge-Ganuzas et al., 2013; Toffolon & Crosato, 2007; Winterwerp et al., 2001) is similar to concept of mutually evasive transport paths (e.g., Dalrymple & Choi, 2007; Dalrymple et al., 1990; Harris, 1988; Harris et al., 2004; Ludwick, 1975; Wells, 1995). The latter, for example, occurs around elongated tidal bars, where the opposite sides of the bar crest have opposing directions of residual sand transport and residual water flow, forming a circulation pattern. The difference between the latter and former group of authors is that the macrocells describe only the largest scale of bars, whereas the mutually evasive transport paths occur at a range of scales, including that of the smallest shoals as also observed in experiments (Kleinhans, Scheltinga, et al., 2015; Kleinhans et al., 2014).

The experimental results in this study show that already after 800 tidal cycles serial circulation cells have evolved and that these circulation patterns can be used to explain how forced midchannel bars cause bank erosion (Figures 7a and 7b). After the experimental estuary became wide enough, a pattern with parallel circulation cells or cells with a mixed coupling (Winterwerp et al., 2001) evolved (Figures 7c and 7e). Later phases of the experiment illustrated that the boundary of two successive circulation cells typically occurred at a major confluence and at locations where the estuary width is relatively narrow. The length of circulation cells scales with bar length, and both bar length and circulation cell length correlate with estuary width (Figures 10b–10d). These patterns resemble the patterns observed in the Western Scheldt (Figure 13 and supporting information Figure S6).

4.4. Cyclicity of Channels and Bars in Tidal Systems

Cyclicity is the periodic migration of channels and bars, in which the original configuration reoccurs after a given period. This has previously been reported for natural tidal systems as well as experiments. For example, experiments of short tidal basins show periodic migration of channels and shoals, which is coupled to reorganization of the channels in the tidal basin (Kleinhans et al., 2015). Most of the studies so far focussed on cyclicity on the ebb tidal delta (e.g., Elias & van der Spek, 2006; Israel & Dunsbergen, 1999; Oost, 1995), on which channels migrate from one side to the other, after which they disappear and reappear at their initial position. However, besides ebb deltas and the quasi-cyclic morphologic behavior of the smaller-scale connecting channels that link the large ebb and flood channels in macro cells (de Vriend et al., 2011; Jeuken, 2000; Swinkels et al., 2009; Toffolon & Crosato, 2007; van den Berg et al., 1996; van Veen, 1950), little is known about the cyclicity of bars and channels within tidal basins or estuaries.

Levoy et al. (2017) observed an 18.6-year cycle in the migration of channels and tidal flats in the bay of Mont-Saint-Michel (France). They state that the periodic increase and decrease in flood dominance correspond with the periodic shift in the location of the channel, which is either located in the north or the south of the embayment. In this case, the bayward migration of tidal sand ridges forced a change in the inflow and outflow directions of the tidal channels. It is hypothesized that a progressively northward swing of the northern channel configuration is caused by sand choking, that is, a large sediment supply partly blocking the main channel. This latter mechanism could be similar to the observations in the final stage of the scale experiments, in which the ebb tidal delta progressively expands in landward direction, followed by a southward migration of the channel at 11–12 m (supporting information Figures S2s–S2u).

While not explicitly stated in the original paper (Levoy et al., 2017), the presence of a monastery and some local bedrock in the middle of the entrance of the embayment may have had a forcing effect on the inflow location and direction of the tidal channels. Similarly, the local confinement present eastward in the embayment could force the main confluence location there. The observation in our experiments, where major confluences and narrow zones in the outline are self-formed thus fits with observations in this natural system. In addition, Levoy et al. (2017) recorded that infill of channels by reworking of bar sediments can cause sudden shifts of channels, which was also observed in the experiments when an ebb channel progressively blocks the evading flood channel by forming a u-shaped bar into that channel.

Our experimental results suggest that without any human interference (e.g., dredging or bank protection), the morphodynamics of macrocells remain active: the roles and locations of ebb and flood tidal channels may reverse within approximately 1,000 tidal cycles and intertidal bars between these channels are continuously reworked. This is in contrast with natural systems under human interferences, in which dredging may cause degeneration of the affected cell and subsequently evolve into a single-channel system (Jeuken & Wang, 2010; Wang et al., 2015; Wang & Winterwerp, 2001) and for which smaller connecting channels are disappearing by marsh formation on top of the shoals (Swinkels et al., 2009). Open questions include what the effect of dredging and dumping will be on the morphodynamics of estuaries and how an engineered estuary compares to a reference case with exactly the same initial and boundary conditions but without any human interference.

5. Conclusions

An experiment in a periodic tilting flume revealed the long-term evolution of channel and bar patterns in self-formed estuaries. Typically, in the landward part a stable meandering channel forms, whereas in the seaward part dynamic channels and bars form that periodically shift laterally. The estuary banks are eroded in phases when forced midchannel bars are present, which results in an estuary planform that is locally wider than the ideal converging shape. Zones with abundant and dynamic bars are separated by locations of channel confluences. We conclude that stable confluence locations in self-formed estuaries are controlled by the spacing of tidal bars, which both are a function of estuary width. The channels between the stable confluences are highly dynamic, which results in a quasiperiodic estuary planform.

The self-formed experimental estuary specifically shows that major confluences occur at relatively narrow parts in the outline and that these confinements are self-formed by sidebar formation. This corresponds to observations in natural systems in which major confluences also occur at self-formed confinements, for example, by salt marsh formation, as well as at forced confinements, for example, by inherited geology or human engineering. However, natural channels and bars are limited in their dynamics, because channels are largely fixed or maintained in place. While the ideal estuary shape may be applicable to tidal creeks and branches of

deltas in equilibrium, the experimental results and observations in natural systems suggest that in self-formed alluvial estuaries in absence of any external forcing (geology and human influence) an autogenically formed quasiperiodic estuary planform evolves.

Acknowledgments
This research was supported by the Dutch Technology Foundation TTW (grant Vici 016.140.316/13710 to M. G. K., which is part of the Netherlands Organisation for Scientific Research (NWO and is partly funded by the Ministry of Economic Affairs). This work is part of the PhD research of J. R. F. W. L. and L. B. Detailed reviews by Bob Dalrymple, one anonymous reviewer, and steer by the Editor and Associate Editor helped to improve the manuscript. We are grateful for technical support by Marcel van Maarseveen, Chris Roosendaal, Henk Markies, and Arjan van Eijk. The authors contributed in the following proportions to conception and design, data collection and processing, analysis and conclusions, and manuscript preparation: J. R. F. W. L.(55%, 45%, 75%, and 75%), L. B. (5%, 45%, 0%, and 0%), W. M. v. D. (5%, 5%, 10%, and 10%), T. d. H.(5%, 5%, 5%, and 5%), and M. G. K. (30%, 0%, 10%, and 10%). E. P. v. O. conducted scaled gravity wave experiments in the Metronome and analyzed the resulting data as part of his MSc research and BGR contributed to conception and design of the wave scaling. The data used are listed in the references, figures, and supporting information.

References

Agisoft, L. (2017). Agisoft photoscan.
Ashmore, P. E. (2001). *Gravel-bed river V, chap. braiding phenomena: Statics and kinetics* (pp. 95–114), Wellington: New Zealand Hydrological Society Inc.
Ashworth, P. J., Best, J. L., Roden, J. E., Bristow, C. S., & Klaassen, G. J. (2000). Morphological evolution and dynamics of a large, sand braid-bar, Jamuna River, Bangladesh. *Sedimentology*, *47*(3), 533–555.
Baar, A., de Smit, J., Uijttewaal, W., & Kleinhans, M. (2018). Sediment transport of fine sand to fine gravel on transverse bed slopes in rotating annular flume experiments. *Water Resources Research*, *54*, 19–45. https://doi.org/10.1002/2017WR020604
Bartels, P. (2015). Ups-and-downs of tidal systems: Formation and development of ebb-and flood tidal channels and bars. (Master's thesis), Utrecht University.
Braat, L., Leuven, J. R. F. W., Lokhorst, I. R., & Kleinhans, M. G. (2018). Effects of estuarine mudflat formation on tidal prism and large-scale morphology in experiments. *Earth Surface Processes and Landforms*. https://doi.org/10.1002/esp.4504
Braat, L., van Kessel, T., Leuven, J. R. F. W., & Kleinhans, M. G. (2017). Effects of mud supply on large-scale estuary morphology and development over centuries to millennia. *Earth Surface Dynamics*, *5*, 617–652. https://doi.org/10.5194/esurf-5-617-2017
Bridge, J. (2003). *Rivers and floodplains* (491 pp.). Malden, MA: Blackwell Publishing.
Chandler, J. H., Shiono, K., Rameshwaren, P., & Lane, S. N. (2001). Measuring flume surfaces for hydraulics research using a Kodak DCS460. *The Photogrammetric Record*, *17*(97), 39–61.
Cleveringa, J. (2013). Ontwikkeling mesoschaal westerschelde - instandhouding vaarpassen schelde milieuvergunningen terugstorten baggerspecie (in dutch) (*Tech. rep.*). Zwolle, NL: ARCADIS.
Dalrymple, R. W., & Choi, K. (2007). Morphologic and facies trends through the fluvial-marine transition in tide-dominated depositional systems: A schematic framework for environmental and sequence-stratigraphic interpretation. *Earth-Science Reviews*, *81*(3), 135–174. https://doi.org/10.1016/j.earscirev.2006.10.002
Dalrymple, R. W., Knight, R., Zaitlin, B. A., & Middleton, G. V. (1990). Dynamics and facies model of a macrotidal sand-bar complex, Cobequid BaySalmon River estuary (Bay of Fundy). *Sedimentology*, *37*(4), 577–612.
Dalrymple, R. W., & Rhodes, R. N. (1995). Estuarine dunes and bars. *Geomorphology and sedimentology of estuaries*, *53*, 359–422.
Dalrymple, R. W., Zaitlin, B. A., & Boyd, R. (1992). Estuarine facies models: Conceptual basis and stratigraphic implications: Perspective. *Journal of Sedimentary Research*, *62*(6), 1130–1146. https://doi.org/10.1306/D4267A69-2B26-11D7-8648000102C1865D
Davis, R. A., & Hayes, M. O. (1984). What is a wave-dominated coast? *Marine geology*, *60*(1-4), 313–329. https://doi.org/10.1016/0025-3227(84)90155-5
de Haas, T., Pierik, H., van der Spek, A., Cohen, K., van Maanen, B., & Kleinhans, M. (2017). Holocene evolution of tidal systems in the netherlands: Effects of rivers, coastal boundary conditions, eco-engineering species, inherited relief and human interference. *Earth-Science Reviews*, *177*, 139–163. https://doi.org/10.1016/j.earscirev.2017.10.006
de Vriend, H. J., Wang, Z. B., Ysebaert, T., Herman, P. M., & Ding, P. (2011). Eco-morphological problems in the Yangtze Estuary and the Western Scheldt. *Wetlands*, *31*(6), 1033–1042. https://doi.org/10.1007/s13157-011-0239-7
Eke, E. (2014). Numerical modeling of river migration incorporating erosional and depositional bank processes (Ph.D. thesis). Urbana, IL: University of Illinois at Urbana-Champaign.
Elias, E. P., & van der Spek, A. J. (2006). Long-term morphodynamic evolution of Texel inlet and its ebb-tidal delta (the Netherlands). *Marine Geology*, *225*(1), 5–21.
Elias, E. P., van der Spek, A. J., & Lazar, M. (2017). The oordelta the contiguous ebb-tidal deltas in the SW Netherlands: Large-scale morphological changes and sediment budget 1965–2013; impacts of large-scale engineering. *Netherlands Journal of Geosciences*, *96*(3), 233–259.
Fonstad, M. A., Dietrich, J. T., Courville, B. C., Jensen, J. L., & Carbonneau, P. E. (2013). Topographic structure from motion: A new development in photogrammetric measurement. *Earth Surface Processes and Landforms*, *38*(4), 421–430.
Harris, P. T. (1988). Large-scale bedforms as indicators of mutually evasive sand transport and the sequential infilling of wide-mouthed estuaries. *Sedimentary Geology*, *57*(3-4), 273–298.
Harris, P. T., Hughes, M. G., Baker, E. K., Dalrymple, R. W., & Keene, J. B. (2004). Sediment transport in distributary channels and its export to the pro-deltaic environment in a tidally dominated delta: Fly river, Papua New Guinea. *Continental Shelf Research*, *24*(19), 2431–2454.
Hijma, M. P., & Cohen, K. M. (2011). Holocene transgression of the Rhine river mouth area, The Netherlands/Southern North Sea: Palaeogeography and sequence stratigraphy. *Sedimentology*, *58*(6), 1453–1485.
Hundey, E., & Ashmore, P. (2009). Length scale of braided river morphology. *Water Resources Research*, *45*, W08409. https://doi.org/10.1029/2008WR007521
Ikeda, S., & Parker, G. (1989). *River meandering*: American Geophysical Union.
Israel, C., & Dunsbergen, D. (1999). Cyclic morphological development of the Ameland Inlet, The Netherlands. In *Proceedings of Symposium on River, Coastal and Estuarine Morphodynamics (Genova, Italy)* (Vol. 2, pp. 705–714).
Jeuken, M.-C. J. L. (2000). *On the morphologic behaviour of tidal channels in the Westerschelde Estuary*. Utrecht, NL: Utrecht University.
Jeuken, M., & Wang, Z. (2010). Impact of dredging and dumping on the stability of ebb-flood channel systems. *Coastal Engineering*, *57*(6), 553–566.
Kleinhans, M. G., Braudrick, C., Van Dijk, W. M., Van de Lageweg, W. I., Teske, R., & Van Oorschot, M. (2015). Swiftness of biomorphodynamics in lilliput-to giant-sized rivers and deltas. *Geomorphology*, *244*, 56–73.
Kleinhans, M. G., Leuven, J. R., Braat, L., & Baar, A. (2017). Scour holes and ripples occur below the hydraulic smooth to rough transition of movable beds. *Sedimentology*, *64*, 1381–1401.
Kleinhans, M. G., Scheltinga, R. T., Vegt, M., & Markies, H. (2015). Turning the tide: Growth and dynamics of a tidal basin and inlet in experiments. *Journal of Geophysical Research: Earth Surface*, *120*, 95–119. https://doi.org/10.1002/2014JF003127
Kleinhans, M., Van Rosmalen, T., Roosendaal, C., & van der Vegt, M. (2014). Turning the tide: Mutually evasive ebb-and flood-dominant channels and bars in an experimental estuary. *Advances in Geosciences*, *39*, 21–26.
Kleinhans, M. G., & van den Berg, J. H. (2011). River channel and bar patterns explained and predicted by an empirical and a physics-based method. *Earth Surface Processes and Landforms*, *36*(6), 721–738. https://doi.org/10.1002/esp.2090

Kleinhans, M. G., van der Vegt, M., Leuven, J., Braat, L., Markies, H., Simmelink, A., et al. (2017). Turning the tide: Comparison of tidal flow by periodic sealevel fluctuation and by periodic bed tilting in the metronome tidal facility. *Earth Surface Dynamics Discussions*, *2017*, 1–35. https://doi.org/10.5194/esurf-2017-11

Kleinjan, I. (1938). Het gebied van de westerschelde nabij bath. Rapport R88a, 88b, 88c. Rijkswaterstaat, Dordrecht.

Lane, S., Richards, K., & Chandler, J. (1993). Developments in photogrammetry: The geomorphological potential. *Progress in Physical Geography*, *17*(3), 306–328.

Langbein, W. (1963). The hydraulic geometry of a shallow estuary. *Hydrological Sciences Journal*, *8*(3), 84–94. https://doi.org/10.1080/02626666309493340

Lanzoni, S., & Seminara, G. (2006). On the nature of meander instability. *Journal of Geophysical Research*, *111*, F04006. https://doi.org/10.1029/2005JF000416

Leopold, L. B., & Wolman, M. G. (1960). River meanders. *Geological Society of America Bulletin*, *71*(6), 769–793.

Leuven, J. (2014). Turning the tide: The effect of river discharge on estuary dynamics and equilibrium (Master's thesis), Utrecht University.

Leuven, J. R. F. W., de Haas, T., Braat, L., & Kleinhans, M. G. (2018). Topographic forcing of tidal sand bar patterns for irregular estuary planforms. *Earth Surface Processes and Landforms*, *43*, 172–186. https://doi.org/10.1002/esp.4166

Leuven, J. R. F. W., Kleinhans, M. G., Weisscher, S. A. H., & van der Vegt, M. (2016). Tidal sand bar dimensions and shapes in estuaries. *Earth-science reviews*, *161*, 204–233. https://doi.org/10.1016/j.earscirev.2016.08.004

Leuven, J. R. F. W., Selaković, S., & Kleinhans, M. G. (2018). Morphology of bar-built estuaries: Empirical relation between planform shape and depth distribution. *Earth Surface Dynamics*, *6*, 763–778. https://doi.org/10.5194/esurf-6-763-2018

Leuven, J. R. F. W., van Maanen, B., Lexmond, B. R., van der Hoek, B. V., Spruijt, M. J., & Kleinhans, M. G. (2018). Dimensions of fluvial-tidal meanders: Are they disproportionally large? *Geology*, *46*(10), 923–926. https://doi.org/10.1130/G45144.1

Levoy, F., Anthony, E., Dronkers, J., Monfort, O., Izabel, G., & Larsonneur, C. (2017). Influence of the 18.6-year lunar nodal tidal cycle on tidal flats: Mont-Saint-Michel Bay, France. *Marine Geology*, *387*, 108–113.

Lokhorst, I., Braat, L., Leuven, J. R. F. W., Baar, A. W., van Oorschot, M., Selaković, S., & Kleinhans, M. G. (2018). Morphological effects of vegetation on the fluvial-tidal transition in holocene estuaries. *Earth Surface Dynamics Discussions*, *2018*, 1–28. https://doi.org/10.5194/esurf-2018-29

Ludwick, J. C. (1975). Tidal currents, sediment transport, and sand banks in Chesapeake Bay Entrance, Virginia, *Geology and engineering* (pp. 365–380). Elsevier. https://doi.org/10.1016/B978-0-12-197502-9.50027-7

Manning, A. (2007). Enhanced UK estuaries database: Explanatory notes and metadata (*Tech. Rep. TR167*). UK: HR Wallingford Tech. Report, TR167.

Mayor-Mora, R. E. (1977). Laboratory investigation of tidal inlets on sandy coasts. California University, Berkeley Hydraulic Engineering Lab.

Monge-Ganuzas, M., Cearreta, A., & Evans, G. (2013). Morphodynamic consequences of dredging and dumping activities along the lower Oka estuary (Urdaibai Biosphere Reserve, southeastern Bay of Biscay, Spain). *Ocean & Coastal Management*, *77*, 40–49.

Morgan, J. A., Brogan, D. J., & Nelson, P. A. (2017). Application of structure-from-motion photogrammetry in laboratory flumes. *Geomorphology*, *276*, 125–143.

Mori, N., & Chang, K.-A. (2003). Experimental study of a horizontal jet in a wavy environment. *Journal of Engineering Mechanics*, *129*(10), 1149–1155.

Oost, A. P. (1995). Dynamics and sedimentary developments of the Dutch Wadden Swith a special emphasis on the Frisian Inlet: A study of the barrier islands, ebb-tidal deltas, inlets and drainage basins (Ph.D. thesis), Utrecht University.

Parker, G., Shimizu, Y., Wilkerson, G., Eke, E. C., Abad, J. D., Lauer, J., et al. (2011). A new framework for modeling the migration of meandering rivers. *Earth Surface Processes and Landforms*, *36*(1), 70–86. https://doi.org/10.1002/esp.2113

Pierik, H., Cohen, K., Vos, P., van der Spek, A., & Stouthamer, E. (2017). Late holocene coastal-plain evolution of the Netherlands: The role of natural preconditions in human-induced sea ingressions. *Proceedings of the Geologists' Association*, *128*(2), 180–197.

Pillsbury, G. (1956). Tidal hydraulics. Revised edition, corps of engineers. US Army, May.

Repetto, R., & Tubino, M. (2001). Topographic expressions of bars in channels with variable width. *Physics and Chemistry of the Earth, Part B: Hydrology, Oceans and Atmosphere*, *26*(1), 71–76.

Reynolds, O. (1887). On certain laws relating to the regime of rivers and on the possibüity of experiments at small scale.

Reynolds, O. (1889). On model estuaries in report of the committee appointed to investigate the action of waves and currents on the beds and fore shores of estuaries by means of working models. *Report of the British Association*, 327–343.

Savenije, H. H. (2015). Prediction in ungauged estuaries: An integrated theory. *Water Resources Research*, *51*, 2464–2476. https://doi.org/10.1002/2015WR016936

Schuurman, F., & Kleinhans, M. G. (2015). Bar dynamics and bifurcation evolution in a modelled braided sand-bed river. *Earth Surface Processes and Landforms*, *40*(10), 1318–1333.

Schuurman, F., Marra, W. A., & Kleinhans, M. G. (2013). Physics-based modeling of large braided sand-bed rivers: Bar pattern formation, dynamics, and sensitivity. *Journal of Geophysical Research: Earth Surface*, *118*, 2509–2527. https://doi.org/10.1002/2013JF002896

Schuurman, F., Shimizu, Y., Iwasaki, T., & Kleinhans, M. (2016). Dynamic meandering in response to upstream perturbations and floodplain formation. *Geomorphology*, *253*, 94–109.

Schuurman, F., Ta, W., Post, S., Sokolewicz, M., Busnelli, M., & Kleinhans, M. (2018). Response of braiding channel morphodynamics to peak discharge changes in the upper yellow river. *Earth Surface Processes and Landforms*, *43*, 1648–1662. https://doi.org/doi.org/10.1002/esp.4344

Seminara, G. (2010). Fluvial sedimentary patterns. *Annual Review of Fluid Mechanics*, *42*, 43–66.

Stefanon, L., Carniello, L., D'Alpaos, A., & Lanzoni, S. (2010). Experimental analysis of tidal network growth and development. *Continental Shelf Research*, *30*(8), 950–962.

Struiksma, N., Olesen, K., Flokstra, C., & De Vriend, H. (1985). Bed deformation in curved alluvial channels. *Journal of Hydraulic Research*, *23*(1), 57–79.

Swinkels, C. M., Jeuken, C. M., Wang, Z. B., & Nicholls, R. J. (2009). Presence of connecting channels in the Western Scheldt estuary. *Journal of Coastal Research*, *25*, 627–640.

Tambroni, N., Bolla Pittaluga, M., & Seminara, G. (2005). Laboratory observations of the morphodynamic evolution of tidal channels and tidal inlets. *Journal of Geophysical Research*, *110*, F04009. https://doi.org/10.1029/2004JF000243

Tambroni, N., Luchi, R., & Seminara, G. (2017). Can tide dominance be inferred from the point bar pattern of tidal meandering channels? *Journal of Geophysical Research: Earth Surface*, *122*, 492–512. https://doi.org/10.1002/2016JF004139

Toffolon, M., & Crosato, A. (2007). Developing macroscale indicators for estuarine morphology: The case of the Scheldt estuary. *Journal of Coastal Research*, *23*(1), 195–212.

Townend, I. (2012). The estimation of estuary dimensions using a simplified form model and the exogenous controls. *Earth Surface Processes and Landforms*, *37*(15), 1573–1583. https://doi.org/10.1002/esp.3256

Tubino, M., Repetto, R., & Zolezzi, G. (1999). Free bars in rivers. *Journal of Hydraulic Research*, *37*(6), 759–775.

van Dijk, W. M., Lageweg, W. I., & Kleinhans, M. G. (2013). Formation of a cohesive floodplain in a dynamic experimental meandering river. *Earth Surface Processes and Landforms*, *38*(13), 1550–1565.

van Dijk, W. M., van de Lageweg, W. I., & Kleinhans, M. G. (2012). Experimental meandering river with chute cutoffs. *Journal of Geophysical Research*, *117*, F03023. https://doi.org/10.1029/2011JF002314

van Veen, J. (1944). Schelderegiem en schelderegie (*Tech. rep.*) Middelburg: Rijkswaterstaat reprint 1993.

van Veen, J. (1950). Eb-en vloedschaarsystemen in de nederlandse getijwateren. *Tijdschrift Koninklijk Nederlands Aardrijkskundig Genootschap*, *67*, 303–325.

van de Lageweg, W. I., van Dijk, W. M., Baar, A. W., Rutten, J., & Kleinhans, M. G. (2014). Bank pull or bar push: What drives scroll-bar formation in meandering rivers? *Geology*, *42*(4), 319–322.

van den Berg, J. H., Jeuken, C. J., & Van der Spek, A. J. (1996). Hydraulic processes affecting the morphology and evolution of the Westerschelde estuary. In J. H. van den Berg, C. J. Jeuken, & A. J. Van der Spek (Eds.), *Estuarine shores: Evolution, environments and human alterations* (pp. 157–184). London, UK: John Wiley.

van der Spek, A. J., & Beets, D. J. (1992). Mid-holocene evolution of a tidal basin in the Western Netherlands: A model for future changes in the Northern Netherlands under conditions of accelerated sea-level rise? *Sedimentary geology*, *80*(3), 185–197.

van der Wegen, M., & Roelvink, J. (2012). Reproduction of estuarine bathymetry by means of a process-based model: Western Scheldt case study, The Netherlands. *Geomorphology*, *179*, 152–167. https://doi.org/10.1016/j.geomorph.2012.08.007

Vlaswinkel, B. M., & Cantelli, A. (2011). Geometric characteristics and evolution of a tidal channel network in experimental setting. *Earth Surface Processes and Landforms*, *36*(6), 739–752.

Wang, Z., Van Maren, D., Ding, P., Yang, S., Van Prooijen, B., De Vet, P., et al. (2015). Human impacts on morphodynamic thresholds in estuarine systems. *Continental Shelf Research*, *111*, 174–183.

Wang, Z., & Winterwerp, J. (2001). Impact of dredging and dumping on the stability of ebb-flood channel systems. In *Proceedings of the 2nd IAHR symposium on River, Coastal and Estuarine Morphodynamics* (pp. 515–524). Obihiro, Japan.

Wells, J. T. (1995). Tide-dominated estuaries and tidal rivers. In *Developments in sedimentology* (Vol. 53, pp. 179–205). Elsevier. https://doi.org/10.1016/S0070-4571(05)80026-3

Westoby, M., Brasington, J., Glasser, N., Hambrey, M., & Reynolds, J. (2012). Structure-from-motion photogrammetry: A low-cost, effective tool for geoscience applications. *Geomorphology*, *179*, 300–314.

Winterwerp, J., Wang, Z., Stive, M., Arends, A., Jeuken, C., Kuijper, C., & Thoolen, P. (2001). A new morphological schematization of the Western Scheldt estuary, The Netherlands. In *Proceedings of the 2nd IAHR symposium on River, Coastal and Estuarine Morphodynamics* (pp. 525–533). Obihiro, Japan.

Wu, F.-C., Shao, Y.-C., & Chen, Y.-C. (2011). Quantifying the forcing effect of channel width variations on free bars: Morphodynamic modeling based on characteristic dissipative Galerkin scheme. *Journal of Geophysical Research*, *116*, F03023. https://doi.org/10.1029/2010JF001941

Yalin, M. (1971). On the formation of dunes and meanders. In *Proceedings of the 14th Congress of the International Association for Hydraulic Research*, *3* (pp. 101–108). Paris, France.

Zolezzi, G., Luchi, R., & Tubino, M. (2012). Modeling morphodynamic processes in meandering rivers with spatial width variations. *Reviews of Geophysics*, *50*, RG4005. https://doi.org/10.1029/2012RG000392